Mathematical models to investigate the relationship between cross-immunity and replacement of influenza subtypes

by

S M Asaduzzaman
B.Sc., University of Dhaka, 2006
M.Sc., University of Dhaka, 2008
M.Sc., University of Western Ontario, 2011

A Dissertation Submitted in Partial Fulfillment of the
Requirements for the Degree of

DOCTOR OF PHILOSOPHY

in the Department of Mathematics and Statistics

Mathematical models to investigate the relationship between cross-immunity and replacement of influenza subtypes

by

S M Asaduzzaman
B.Sc., University of Dhaka, 2006
M.Sc., University of Dhaka, 2008
M.Sc., University of Western Ontario, 2011

Supervisory Committee

Dr. Junling Ma, Co-Supervisor
(Department of Mathematics and Statistics)

Dr. Pauline van den Driessche, Co-Supervisor
(Department of Mathematics and Statistics)

Dr. Steve Perlman, Outside Member
(Department of Biology)

ABSTRACT

A pandemic subtype of influenza A sometimes replaces (e.g., in 1918, 1957, 1968) but sometimes coexists (e.g., in 1977) with the previous seasonal subtype. This research aims to determine a condition for replacement or coexistence of influenza subtypes. We formulate a hybrid model for the dynamics of influenza A epidemics taking into account cross-immunity of influenza strains depending on the most recent seasonal infection. A combination of theoretical and numerical analyses shows that for very strong cross-immunity between seasonal and pandemic subtypes, the pandemic cannot invade, whereas for strong and weak cross-immunity there is coexistence, and for intermediate levels of cross-immunity the pandemic may replace the seasonal subtype.

Cross-immunity between seasonal strains is also a key factor of our model because it has a major influence on the final size of seasonal epidemics, and on the distribution of susceptibility in the population. To determine this cross-immunity, we design a novel statistical method, which uses a theoretical model and clinical data on attack rates and vaccine efficacy among school children for two seasons after the 1968 A/H3N2 pandemic. This model incorporates the distribution of susceptibility and the dependence of cross-immunity on the antigenic distance of drifted strains. We find that the cross-immunity between an influenza strain and the mutant that causes the next epidemic is 88%. Our method also gives an estimated value 2.15 for the basic reproduction number $\mathcal{R}_0$ of the 1968 pandemic influenza.

Our hybrid model agrees qualitatively with the observed subtype replacement or coexistence in 1957, 1968 and 1977. However, our model with the homogeneous mixing assumption significantly over estimates the pandemic attack rate. Thus, we modify the model to incorporate heterogeneity in the contact rate of individuals. Using the determined values of cross-immunity and $\mathcal{R}_0$, this modification lowers the pandemic attack rate slightly, but it is still higher than the observed attack rates.

Contents

List of Tables

List of Figures

ACKNOWLEDGEMENTS

I would like to thank:

My wife, for her constant help and support, and **my daughter** who sacrificed a lot of her play time for me.

My supervisors Dr. Junling Ma and Dr. Pauline van den Driessche, for their mentoring, support, encouragement, and patience.

Graduate students in the Department of Mathematics and Statistics, for a friendly environment to work and play.

University of Victoria, for funding me with a scholarship.

DEDICATION

To my beloved daughter **Anaum Ammara**.

Chapter 1

Introduction

1.1 Influenza

Influenza is an important cause of morbidity and mortality in humans [34]. Seasonal influenza accounts for more than 41,000 deaths each year in North-America [33], whereas the 1918 influenza pandemic is estimated to have caused approximately 50 million deaths worldwide [73]. Influenza, an upper respiratory infection in humans, is caused by an RNA virus in the family of Orthomyxoviridae [34]. The symptoms of influenza infection are characterized by the sudden onset of fever, cough, and sneezing. Deaths due to influenza are a small percentage of infection; infected individuals usually recover naturally [25]. Influenza virus in humans is mainly of three types: A, B and C. Influenza virus type A is found in a variety of avians and mammals, type B is mainly found in humans, and very little is known about influenza type C [34]. Influenza virus types are distinguished by the differences of two surface proteins – hemagglutinin (HA) and neuraminidase (NA) [78]. Influenza virus type A is further divided into subtypes based on the surface proteins HA and NA. Two subtypes H1N1 and H3N2 are currently circulating in humans.

Seasonal influenza epidemics emerge in the winter. Thus there are two seasonal influenza seasons worldwide corresponding to the occurrence of the winter season in the Northern and Southern hemispheres. The effects of influenza are either direct or indirect on a host. The direct effects include destruction of infected cells, damage to respiratory epithelium and immunological responses that cause malaise and pneumonia, and indirect effects include secondary bacterial infections as a result of tissue damage [64].

1.2 Reservoirs of Influenza

Aquatic birds are the natural reservoir of all the subtypes of influenza A virus. Avian influenza viruses have been isolated from freshly deposited fecal materials [79]. Pigs and horses are probably infected by avian influenza virus through fecal-oral contamination of water [77]. Feeding pigs, with untreated garbage or carcasses of dead birds may contribute to the transmission of avian influenza virus to pigs [66]. The isolation of H5N2 influenza virus from pigs living under chicken houses supports the direct transmission of influenza virus from birds to pigs [77]. After transmission from birds to mammals, the method of spread of transmission is mainly respiratory. All mammalian influenza viruses have originated from the avian influenza reservoir [77] and have caused outbreaks in mammals including seals [50], whales [49], pigs [65] and domestic poultry [47].

1.3 Evolution of Influenza

Influenza virus undergoes two types of evolution: antigenic drift (point mutation) and antigenic shift (gene reassortment) [34, 77]. Antigenic drift is a rapid minor genetic variation in currently circulating subtypes [71]. Due to antigenic drift, influenza virus subtypes have many strains. The evolutionary root of influenza strains from a common ancestor is depicted by the branching in the phylogenetic tree (see Fig. 1.1), in which two influenza strains are more related if they have a more recent common ancestor. The occurrence and severity of recurrent annual influenza epidemic outbreaks are driven by viral antigenic drifts [71]. Without antigenic drifts, human influenza viruses would disappear once the herd immunity had reached a critical threshold [70]. Influenza virus drifts away from recognition by the immune system avoiding much population immunity; thus there remain sufficient susceptible individuals to support subsequent epidemics [30, 38, 61].

The immunological change that produces a naive virus isolate is known as antigenic shift, which usually results from the recombination of gene segments from viruses circulating in humans with virus segments from avian viruses [10]. Pigs are believed to be the mixing vessel for the combination of gene segments because both the human and avian influenza viruses can infect pigs in suitable condition [15]. Nucleotide sequencing of the 1957 pandemic revealed that five genes were derived from the human H1N1 seasonal influenza, whereas the 1968 pandemic derived six genes from the H2N2 seasonal influenza [78]. In the last century, there were three major genetic shifts of influenza virus causing

FIG. 1.—Maximum-parsimony tree constructed from 357 HA1 genes of the human influenza virus type A subtype H3.

Figure 1.1: Phylogenetic tree of influenza A/H3N2 from Bush et al. [16].

three major pandemics in 1918, 1957 and 1968 to which most humans and swine were immunologically naive [70].

The genetic structure of the 1918 pandemic was obtained using frozen lung tissue from three victims of the 1918 pandemic influenza, showing that the hemagglutinin and neuraminidase surface proteins were derived from avian like influenza virus shortly before the 1918 pandemic, and was not a reassortment of viruses circulating previously in humans [71]. Surprisingly, the avian like influenza viruses were not circulating in humans or pigs for a few decades before the pandemic in 1918. The pandemic influenza virus in 1918 had 8 genome segments significantly different from the ongoing contemporary avian influenza virus genes [73]. Thus, the actual origin of the 1918 pandemic influenza is unknown.

The novel gene segment of the 1957 and 1968 pandemic viruses have all originated in Eurasian avian viruses by the combination of gene segments of Eurasian wild waterfowl strains with previously circulating human influenza strains [10]. All influenza pandemics since 1918 and almost all cases of seasonal influenza A worldwide, with the exception of avian viruses, have been caused by descendants of the 1918 pandemic [70]. The ancestral virus that caused the 1918 pandemic, and the viruses that provided gene segments for the 1957 and 1968 pandemics are still circulating in wild birds with either no or a few mutation changes [77].

1.4 Seasonality of Influenza Epidemics

Seasonal influenza epidemic has been circulating in humans for a long time. Every year a new strain appears and causes an epidemic outbreak, peaking during the winter in temperate regions. Though influenza infection contributes significantly to deaths related to respiratory infection in humans [26], how much mortality is caused by influenza is not know explicitly. According to Centers for Disease Control and Prevention–(i) not all individuals suffering from influenza like symptoms visit a clinic, (ii) individuals may develop a secondary bacterial or viral infection (pneumonia) after an initial infection, and (iii) seasonal influenza can aggravate an existing chronic illness (e.g., congestive heart failure, chronic obstructive pulmonary disease). Thus, many influenza-related deaths are not recorded as influenza, rather as underlying respiratory or chronic conditions. However, influenza-related deaths are considered a good indicator of disease pattern, and are calculated from the number of excess deaths from influenza-related deaths in the winter months in excess of the pneumonia baseline. The baseline is constructed using a seasonal regression approach developed by Serfling in 1963 [68], where a linear regression model with harmonic terms is fitted to non-epidemic weeks to produce the baseline.

The data used to construct Fig. 1.2 is compiled from Canadian Mortality Database. This database contains individual death records in Canada since 1951. We tabulated weekly number of deaths with either pneumonia or influenza (P&I) as a cause of death. Fig. 1.2 shows that the weekly P&I mortality data has peaks in the winter months, exhibiting seasonality in the dynamics of influenza epidemics. The seasonal influenza H1N1, which shows seasonality (Fig. 1.2), was circulating in humans and was replaced by the pandemic H2N2 in 1957; after the pandemic influenza H2N2 continues to circulate in humans and exhibits seasonality (Fig. 1.2).

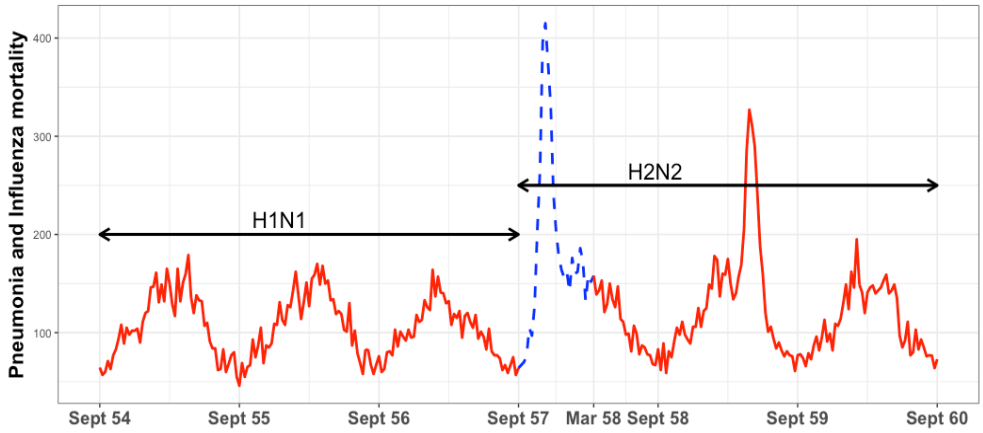

Figure 1.2: Weekly pneumonia and influenza (P&I) mortality data of Canadian population from 1954–1960. The dashed curve shows the P&I deaths during the 1957 pandemic influenza.

1.5 Modeling the Dynamics of Influenza

1.5.1 SIR Model for Single Season Influenza

To understand the dynamics of seasonal influenza, we divide the individuals into classes and model their time rate of transfer from one class to another. This type of model to study the dynamics of diseases is known as a *compartmental model*. The basic compartmental models to describe the transmission of diseases are contained in a sequence of papers by Kermack and McKendrick in 1927, 1932, and 1933 [53–55]. The first of these papers describes epidemic models, which include the dependence on age-of-infection.

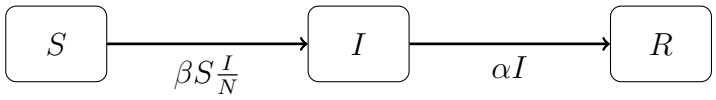

Figure 1.3: The progress of disease dynamics in the SIR model.

We start with a SIR-type model based on Kermack and McKendrick [53–55] epidemic models; individuals are divided into three classes– susceptible (S), infected and infectious (I) and recovered (R). Denote by β the transmission rate from an infectious individual to a susceptible individual and by $\alpha > 0$ the recovery rate. Even though influenza is a major cause of winter mortality, the number of influenza induced deaths is still negligible compared to population size. Thus, we assume that there is no disease death, and neglect birth and death processes for the duration of the seasonal influenza; thus the total population

$N = S + I + R$ is a constant. We do not keep track of changes in the R class as it can be determined from the other equations. Following the model in Fig. 1.3, the dynamics of seasonal influenza can be described by the ordinary differential equations (ODEs)

$$\frac{dS}{dt} = -\beta S\frac{I}{N}, \tag{1.1a}$$
$$\frac{dI}{dt} = \beta S\frac{I}{N} - \alpha I, \tag{1.1b}$$
$$\frac{dR}{dt} = \alpha I. \tag{1.1c}$$

The initial conditions are $S(0) = S_0, I(0) = I_0 \ll N$ is positive and small, and $R(0) = 0$.

The basic reproduction number $\mathcal{R}_0 = \frac{\beta}{\alpha}$ is defined as the expected number of secondary infection from a typical infectious individual introduced in a completely susceptible population. If $\mathcal{R}_0 < 1$, then on average an infectious individual fails to pass on the disease to more than one individual, which fails to cause an epidemic. If $\mathcal{R}_0 > 1$, then on average an infectious individual passes on the disease to more than one individual, which causes an epidemic [31]. The epidemic eventually burns out, i.e., $I(\infty) = 0$ since there is no recruitment in the dynamics of the epidemic.

The positive orthant is invariant; so all solutions of (1.1) lie in the non-negative, bounded set defined by $S, I, R \geq 0$ and $S + I + R = N$. Adding (1.1a) and (1.1b) gives

$$\frac{d}{dt}\big(S + I\big) = -\alpha I \tag{1.2}$$

which is decreasing for $I > 0$. Integrating (1.2) from the beginning of the epidemic at $t = 0$ to the end of the epidemic at $t = \infty$, we obtain

$$S(\infty) - S(0) + I(\infty) - I(0) = -\alpha \int_0^\infty I(t)dt. \tag{1.3}$$

The left side of (1.3) is finite, so $I(\infty) = 0$. Divide (1.1a) by S, and integrate from 0 to ∞ to obtain

$$\log\left(\frac{S(\infty)}{S(0)}\right) = -\frac{\beta}{N}\int_0^\infty I(t)dt$$
$$\log\left(\frac{S(\infty)}{S(0)}\right) = \frac{\beta}{\alpha N}\big[S(\infty) - S(0) + I(\infty) - I(0)\big], \qquad \big[\text{using (1.3)}\big]$$

$$\frac{S(\infty)}{S(0)} = e^{-\frac{\mathcal{R}_0}{N}\left[S(0)-S(\infty)+I(0)-I(\infty)\right]} = e^{-\frac{\mathcal{R}_0}{N}R(\infty)}. \tag{1.4}$$

Thus $S(\infty) > 0$. Denote by $\psi = \frac{S(\infty)}{S(0)}$ the fraction of individuals who escaped influenza infection during the epidemic. The attack rate of influenza, i.e., the fraction of individuals who were infected during the epidemic, is given by $Z = 1 - \psi$; using the attack rate Z, (1.4) simplifies to $Z = 1 - e^{-\mathcal{R}_0 Z}$, which has a unique root in $(0, 1)$ for $\mathcal{R}_0 > 1$.

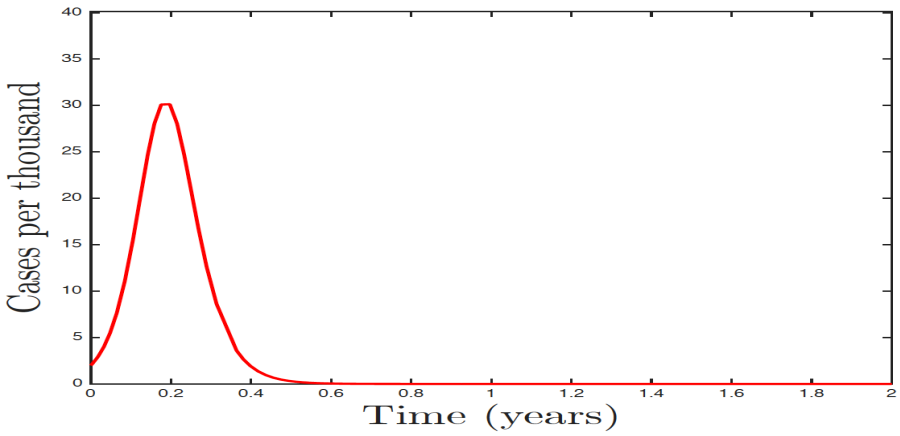

Figure 1.4: The parameters of the model (1.1) are chosen to match the seasonal influenza parameters, i.e., $\mathcal{R}_0 = 1.3$ from Chowell et al. [19], recovery rate $\alpha = 0.2$ per day (infectious period 5 days) and $N = 1000$.

Numerical simulation of the model (1.1) shows that an SIR-type model cannot explain the observed seasonality in the dynamics of seasonal influenza (Fig. 1.4) as there is only one epidemic peak for $\mathcal{R}_0 > 1$, then the epidemic dies out. An SIR-type model does not explain how recovered individuals become susceptible in the next season. However, it can be used to model the dynamics of influenza in a single season. Many authors have used an SIR-type model to study the dynamics of pandemic influenza and the effectiveness of control measures, e.g., vaccination [58], school closures [18] and entry screening [23].

1.5.2 SIRS Model for Endemic Influenza

In order to explain the seasonality of influenza dynamics, we now incorporate the loss of immunity in the SIR-type model to reflect the fact that recovered individuals can become susceptible to influenza virus within a few years [24]. We assume that the recovered individuals can become susceptible at a rate δ to the drifted variants of influenza in the next season. The progress of disease dynamics is depicted in Fig. 1.5.

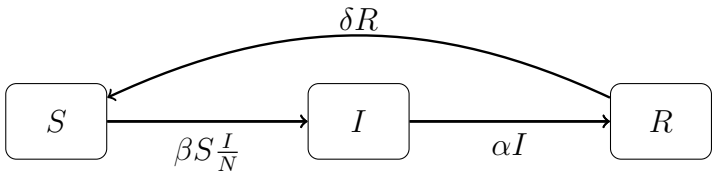

Figure 1.5: The progress of disease dynamics in the SIRS model.

The dynamics of seasonal influenza of the model in Fig. 1.5 evolve according to the ODEs

$$\frac{dS}{dt} = -\beta S\frac{I}{N} + \delta(N - S - I), \tag{1.5a}$$

$$\frac{dI}{dt} = \beta S\frac{I}{N} - \alpha I \tag{1.5b}$$

$$\frac{dR}{dt} = \alpha I. \tag{1.5c}$$

The initial conditions are $S(0) = S_0, I(0) = I_0 \ll N$ is positive and small, and $R(0) = 0$. Numerical simulation of the model (1.5) shows that the SIRS-type model also cannot explain the observed seasonality in the dynamics of seasonal influenza (Fig. 1.6). With these parameter values, for $\mathcal{R}_0 > 1$, the number of cases shows monotonically decreasing oscillations about an endemic equilibrium with $I = 1.6$. The SIRS-type model assumes a constant supply of susceptible individuals due to the loss of immunity; this assumption is not true for seasonal influenza since individuals become susceptible to influenza in the next season because of antigenic drift evolution, not by losing their immunity against influenza.

1.5.3 SIRS Model with Seasonal Forcing on Transmission Rate

It is known that the seasonal forcing on transmission rate β can cause the observed seasonal pattern in the dynamics of influenza epidemics. The transmission rate β changes because of different mixing patterns of individuals over the year, e.g., at the beginning of a school term the contact rate between school aged children suddenly increases, during the winter more time is spent in indoor activities causing an increased contact rate; thus transmission rate β increases [3]. Transmission rate changes can also be caused by the effect of temperature and humidity on transmission [67].

Using a SIRS-type model, the effect of seasonal forcing on β in the dynamics of

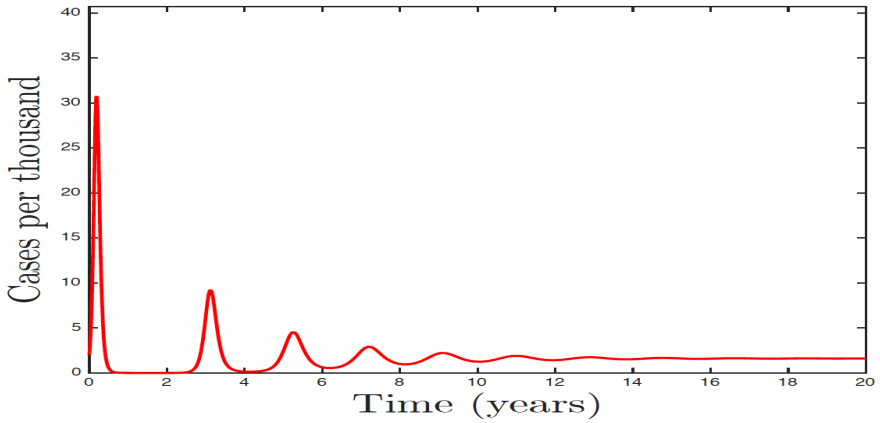

Figure 1.6: The parameters of the model (1.5) are taken to match the seasonal influenza parameters, i.e., $\mathcal{R}_0 = 1.3$ from Chowell et al. [19], recovery rate $\alpha = 0.2$ per day (infectious period 5 days) and rate of immunity loss $\delta = 0.0014$ per day (duration of immunity 2 years) and $N = 1000$.

influenza has been studied by Dushoff et al. [32] by considering a transmission rate $\beta(t)$ that varies sinusoidally, i.e., $\beta(t) = \beta_0[1 + \beta_1 \cos(2\pi t)]$ for some parameters β_0 and β_1. Dushoff et al. [32] showed that the oscillation in influenza incidence can be caused by a small seasonal change in the transmission rate $\beta(t)$. When the period of seasonal forcing $\beta(t)$ is approximately near the period of the model, then resonance may happen to produce greatly amplified oscillations in influenza incidence (Fig. 1.7). A small change in $\beta(t)$, which is very difficult to detect, can cause a large fluctuation in influenza incidence.

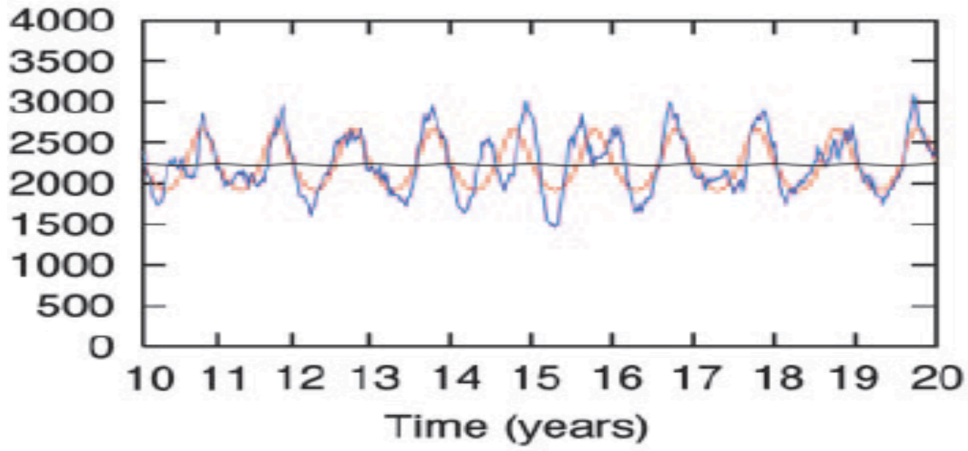

Figure 1.7: The effect of seasonal forcing in the dynamics of influenza from Dushoff et al. [32]. The vertical axis shows the number of influenza cases per $500,000$ individuals. The disease dynamics is simulated with demographic stochasticity (blue curve) and without demographic stochasticity (red curve) .

1.5.4 Two Strain Competition Model

Many authors have looked into other measures such as the effect of *cross-immunity* that cause oscillations in influenza incidence. Cross-immunity is the reduction in the probability of infection to challenging strains. This probability is also called susceptibility. Natural infection give rise to complete immunity to the infecting strain, and partial cross-immunity to the related strains [42, 80]. Influenza vaccine also give rise to cross-immunity [62].

The effect of cross-immunity in the dynamics of influenza epidemics, without any seasonal forcing of the transmission rate, has been studied by Castillo-Chavez et al. [17] using a SIR-type model. Two strains of influenza are assumed to co-circulate in a homogeneous population. It is also assumed that the infection with one strain reduces the susceptibility to the other strain with no co-infection, but the recovered individuals from one strain can get infected with the other strain. The progress of disease dynamics is depicted in Fig. 1.8.

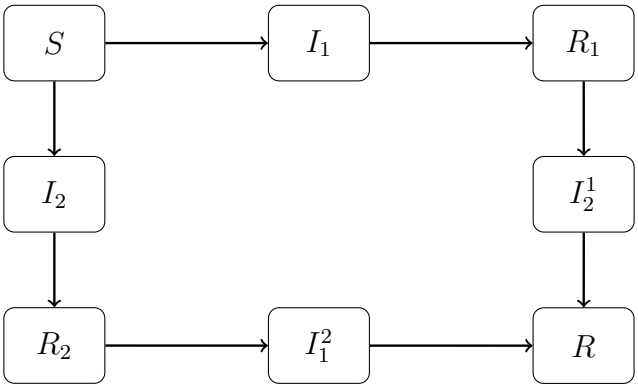

Figure 1.8: The flow of individuals in a homogeneous population when two influenza strains are co-circulating. Here, S: susceptible, I_i: infected by the strain i, R_i: recovered from the strain i, I_i^j: infected by the strain i and recovered from the strain j and R: recovered from both strains.

Following the transfer diagram in Fig. 1.8, the dynamics of influenza epidemics can be

described by the ODEs

$$\frac{dS}{dt} = \mu - \big(\beta_1(I_1 + I_1^2) + \beta_2(I_2 + I_2^1)\big)S - \mu S, \tag{1.6a}$$
$$\frac{dI_i}{dt} = \beta_i(I_i + I_i^j)S - \gamma_i I_i - \mu I_i, \tag{1.6b}$$
$$\frac{dR_i}{dt} = \gamma_i I_i - \sigma_j\beta_j(I_j + I_j^i)R_i - \mu R_i, \tag{1.6c}$$
$$\frac{dI_i^j}{dt} = \sigma_i\beta_i(I_i + I_i^j)R_j - \gamma_i I_i^j - \mu I_i^j, \tag{1.6d}$$
$$\frac{dR}{dt} = \gamma_1 I_1^2 + \gamma_2 I_2^1 - \mu R, \tag{1.6e}$$

where $j = 2$ if $i = 1$ and $j = 1$ if $i = 2$, and the initial conditions of the model are $S(0) = S_0, I_i(0) = I_{i0}, R_i(0) = R_{i0}$, $I_i^j(0) = I_{i0}^j, R(0) = R_0$. Here, S is the susceptible individuals, I_i is the infected individuals by the strain i, R_i is the recovered individuals from the strain i, I_i^j is the infected individuals by the strain i and recovered from the strain j and R is the recovered individuals from both strains. Denote by β_i the transmission coefficient of strain i, by γ_i the recovery rate from strain i, by μ the constant mortality rate, and by σ_i the relative susceptibility to strain i, i.e., $(1 - \sigma_i)$ is the cross-immunity to strain i.

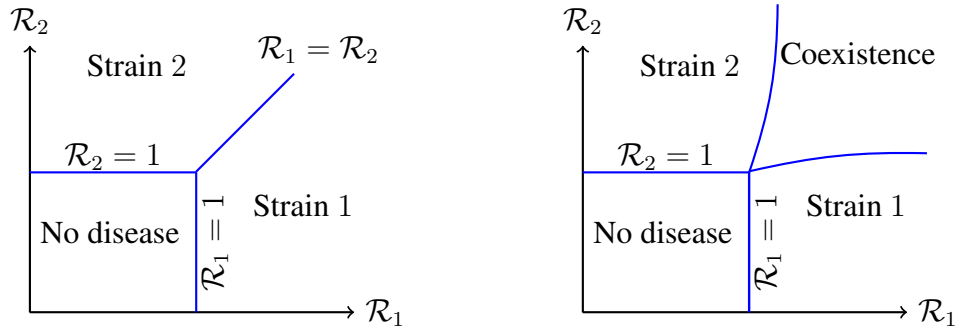

(a) One strain gives complete immunity to the other strain.

(b) Each strain gives some immunity to the other strain.

Figure 1.9: Stability diagram of Castillo-Chavez et al. (1989) model. Here, $\mathcal{R}_i$ is the basic reproduction number of influenza strain i for $i = 1, 2$.

Numerical simulation of the model (1.6) shows that whenever a non-trivial equilibrium exists, it is asymptotically stable (Fig. 1.9), i.e., the two strain model exhibits no sustained oscillation. Though birth and death are included in the model (1.6), the stability of equilibrium points is not dependent on it. Castillo-Chavez et al. [17] also introduced, and analyzed a model that incorporates age structure through age-dependent proportionately

mixed contact rates, age-dependent mortality rates, and interactions among viral strains or subtypes. In the numerical simulation of the age-structure model, Castillo-Chavez et al. [17] found that for sustained oscillations in the dynamics of influenza at least two or more co-circulating viral strains are required.

1.5.5 Infection History Dependent Model: Multi-strain Competition

Andreasen et al. [5] studied the role of cross-immunity for n co-circulating influenza strains in a multi-strain competition modeling framework. An individual's infection history is accounted for by index set notation where the index specifies the set of influenza strains to which the individual was exposed in the past; it is then incorporated in a SIR-type model. For example, an individual's infection history for 3 co-circulating strains belongs to the set $\{\emptyset, \{1\}, \{2\}, \{3\}, \{1,2\}, \{1,3\}, \{2,3\}, \{1,2,3\}\}$. Denote by $S^{\mathcal{L}}$ the number of susceptible individuals with infection history in the set $\mathcal{L}$, $I_i^{\mathcal{L}}$ the number of individuals with infection history $\mathcal{L}$ who are currently infected by the strain i with $i \notin \mathcal{L}$. The follow diagram of individuals is presented in Fig. 1.10.

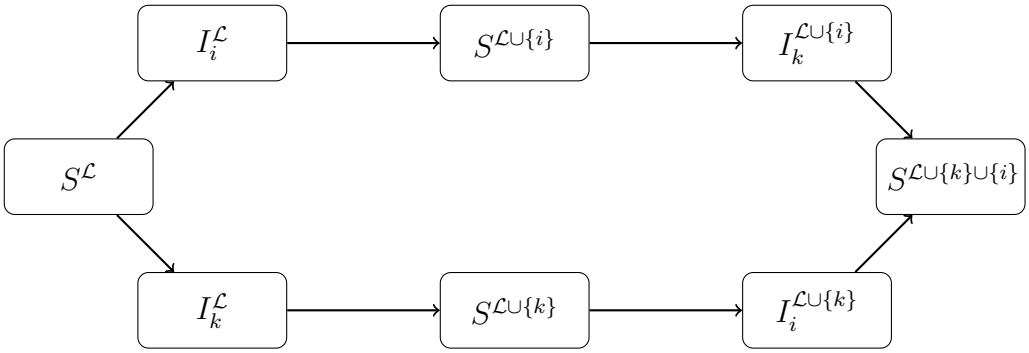

Figure 1.10: The progress of individuals of Andreasen et al. [5] model.

Andreasen et al. [5] assumed that each strain confers some partial cross-immunity to the related strains; cross-immunity reduces the probability of infection (i.e., susceptibility). To keep track of an individual's full infection history, the model required 2^n ODEs to describe the change of susceptible individuals and $n2^{n-1}$ ODEs for the infectious individuals. Theoretical analyses of the model become unmanageable for fairly large number of strains. For $n = 10$, the model requires an analysis of a total of 6144 ODEs. Because of the huge dimensionality, theoretical and numerical analyses are limited to a few strains. Andreasen et al. [5] analyzed their model for four co-circulating strains and found that the model can exhibit sustained oscillations in the disease dynamics for some

parameter values. Thus, the co-occurrence of more strains can give rise to oscillations in the prevalence of disease dynamics.

The Andreasen et al. [5] model has subsequently been used by many authors to study the dynamics of influenza epidemics. Lin et al. [57] used it to study the dynamics of three co-circulating influenza strains, and showed that the interaction among influenza strains conferring partial cross-immunity can give rise to Hopf bifurcation to a periodic solution. Gomes et al. [44] studied the dynamics of influenza by considering the strain-space to be of circular configuration unlike a linear chain configuration as used by Andreasen et al. [5] and Lin et al. [57]. The Andreasen et al. [5] model is also used by other authors, for example, Adams et al. [1], [2]. Because of the huge dimensionality, none of the authors analyzed the model theoretically for a large number of strains; even numerical simulation was limited to a few strains.

1.5.6 Simplified Infection History Dependent Model

Andreasen [4] simplified their previous model as given in section 1.5.5 to seasonal recurrence of influenza epidemics by assuming that an individual's infection history depends only on the most recent infection. Though the phylogenetic tree of influenza A virus shows a branching tree like relation (see section 1.3), the tree is almost linear (that is, no long-term cocirculating branches). Thus, Andreasen [4] assumed a linear structure of the phylogenetic tree.

The linearity assumption on infection history reduces the dimension for n strains from 2^n to only n ODEs to describe the change of susceptible individuals. The time scale of influenza epidemics and viral drift are separated by assuming that each year a new strain appears due to antigenic drift, and all other strains disappear. On the fast time scale, the dynamics of an influenza epidemic was modeled by a SIR-type model. For $i = 1, 2, \ldots, n$ influenza dynamics evolve according to the following ODEs

$$\begin{aligned}
\frac{dS_i}{dt} &= -\lambda\tau_i S_i, \\
\frac{dI_i}{dt} &= \lambda\tau_i S_i - \alpha I_i, \\
\frac{dR_i}{dt} &= \alpha I_i, \\
\lambda &= \beta \sum_{i=1}^{n} \sigma_i I_i
\end{aligned}$$

where the individuals who had seasonal influenza i years before, S_i, I_i and R_i denote susceptible, infectious and recovered individuals in the current season. Denote by τ_i the relative susceptibility and by σ_i the relative infectivity; τ_i and σ_i follow a monotonic increasing relation to incorporate the fact that cross-immunity decreases with time. The parameter λ gives the force of infection on individuals with no immunity to the current strain of influenza. At the end of the epidemic season, the final size relation was found to determine the cross-immunity structure of individuals, which then (on the slow time scale) was related to the beginning of the next season through a discrete mapping.

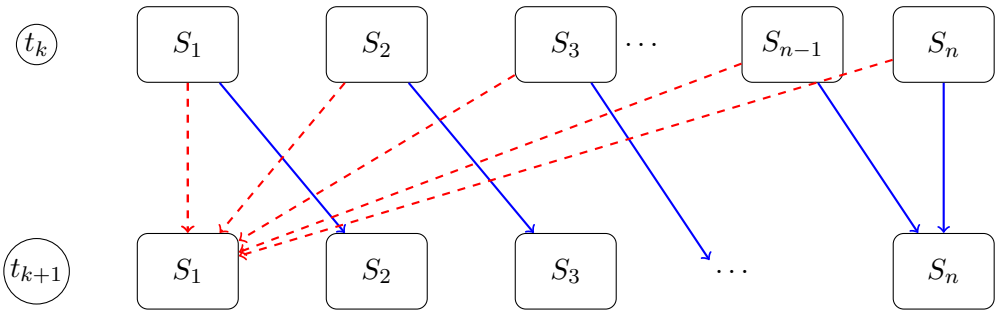

Figure 1.11: The change of immune status of susceptible individuals from the end of the t_k season to the beginning of the t_{k+1} season. The solid and dashed lines are used to represent individuals who escaped and recovered from influenza infection.

The season-to-season mapping equations can be written as

$$\begin{aligned} S_{i+1}(t_{k+1}) &= \phi^{\tau_i} S_i(t_k), \quad i = 1, \ldots, n-2, \\ S_n(t_{k+1}) &= \phi^{\tau_{n-1}} S_{n-1}(t_k) + \phi S_n(t_k), \\ S_1(t_{k+1}) &= 1 - \sum_{i=1}^{n} \phi^{\tau_i} S_i(t_k). \end{aligned}$$

where $\phi = \frac{S_n(\infty)}{S_n(0)}$ is the fraction of individuals from S_n who escaped seasonal influenza infection in the current season. Theoretical and numerical analyses of the mapping equations show that they exhibit sustained oscillations for some parameter values [4].

1.5.7 Modeling Antigenic Drift and Shift

Previous studies on seasonal influenza did not specifically model antigenic drift. Rather, it is assumed that antigenic drift happens and a new strain appears every year. Boni et al. [13] modeled influenza drift assuming that the virus mutates at constant rate. Modeling the drift evolution, Boni et al. (2006) found a condition under which a large amount of

antigenic drift can happen. Following the annual structure of Andreasen's [4] model, Boni et al. [12] modeled influenza drift evolution in a single season, where the antigenic drift depends on the previous year's epidemic size. Ferguson et al. [37] reproduced the drift-like behaviour of influenza A over many seasons using an individual based simulation model, which showed that short-lived cross-immunity restricts viral diversity in the population.

Antigenic shift leading to the emergence of pandemic influenza has been studied by many authors; see for example [6, 29, 81]. Control measures for an emergent pandemic influenza have been studied extensively, e.g., containment at the source [35, 59], antiviral treatment [58], the impact of social distancing [36, 43], school closures [18], travel restrictions [36, 51] and entry screening [23].

1.6 Motivation of the Dissertation

There were major pandemic outbreaks in the last century in $1918, 1957, 1968$ and 1977, and at the beginning of this century in 2009 (Fig. 1.12). The subtype H1N1 that gave rise to the 1918 pandemic influenza [71], existed in humans as a seasonal influenza until 1957, when a new subtype H2N2 emerged and replaced the previously circulating subtype H1N1 [34]. The subtype H2N2 circulated in humans before it was replaced by the subtype H3N2, which emerged from the pandemic influenza in 1968. The replacement of a seasonal subtype by the pandemic subtype was not always the case. The reintroduced pandemic subtype H1N1 in 1977 did not replace the previously circulating subtype H3N2 [34, 78]. Both subtypes coexisted until 2009, when a swine origin pandemic subtype H1N1 replaced the previously circulating seasonal H1N1 and coexisted with H3N2. Despite the existence of a large literature on influenza dynamics, conditions under which a pandemic subtype replaces or coexists with the previous subtype have not so far been considered.

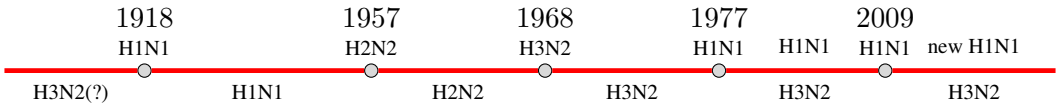

Figure 1.12: Time line of pandemic influenza outbreaks. The numbers correspond to the year of the pandemic influenza outbreak and the subtype names below the numbers are the pandemic subtype that caused pandemic influenza. The subtypes that were circulating before the pandemic outbreak are indicated below (and above) the time line.

1.7 Organization of the Dissertation

The dissertation is organized as follows: Chapter 1 introduces the research problem, some basic mathematical models and a review of mathematical models to study the dynamics of seasonal and pandemic influenza. In Chapter 2, a hybrid model is formulated to study the condition under which a seasonal strain is replaced by or coexists with the pandemic subtype. Following theoretical and numerical analyses of the models, the condition of replacement of a seasonal strain by the pandemic subtype is determined. In Chapter 3, novel statistical model, based on the seasonal model of chapter 2, is designed to determine the cross-immunity between two influenza strains that appear in two consecutive seasons. In Chapter 4, the seasonal model of chapter 2 is adapted to study the dynamics of pandemic influenza, incorporating contact rate heterogeneity of individuals. Chapter 5 revisits the condition under which a seasonal strain is replaced by the pandemic subtype using the parameters (e.g., cross-immunity, basic reproduction number) found in chapter 3, and provides a discussion with possible future research directions. The symbols and their meanings are presented in Appendix A.

Chapter 2

The coexistence or replacement of two subtypes of influenza

2.1 Introduction

Influenza outbreaks occur seasonally in each winter or as pandemic influenza [77], with three major pandemic influenza outbreaks in the last century [34]. A new subtype of influenza virus emerges from a pandemic outbreak and establishes itself in humans, becoming a seasonal influenza virus, and sometimes the current seasonal subtype is replaced by the new pandemic subtype. Fig. 1.12 in section 1.6 shows the time line of pandemic influenza outbreaks. The pandemic influenza H2N2 in 1957 and H3N2 in 1968 replaced previously circulating seasonal subtype, but the pandemic influenza H1N1 in 1977 did not replace the previous subtype (Fig. 1.12). We investigate under what conditions a seasonal subtype can survive in the season after a pandemic or is replaced by the pandemic subtype.

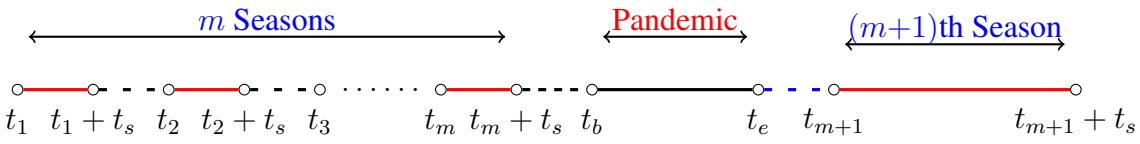

Figure 2.1: Time t_k for $k = 1, 2, \ldots$ denotes the start of a seasonal epidemic with a duration t_s (solid lines). The time between t_k and t_{k+1} is approximately one year. The outbreak of the pandemic influenza starts at time t_b and ends at time t_e. The broken lines indicate no influenza outbreak.

We assume that seasonal influenza has been continuing for many years before the pandemic subtype causes an outbreak. We also assume that the duration of a seasonal

influenza epidemic is t_s. The broken lines in Fig. 2.1 correspond to summer time, and we assume that there is no outbreak of seasonal influenza in the summer. As in Andreasen [4] as given in section 1.5.6, we assume that seasonal and pandemic influenza occur on a fast time scale, whereas the cross-immunity structure changes on a slow time scale. The pandemic influenza starts at time t_b and ends at time t_e (Fig. 2.1), not overlapping with seasonal influenza. After this pandemic, a new strain of the previous season's subtype reappears at time t_{m+1}. The persistence of the seasonal strain in the season after the pandemic is determined by the reproduction number of this seasonal strain at time t_{m+1}.

To determine the reproduction number, we formulate a hybrid model for the interaction of seasonal influenza epidemics and a pandemic following the time line in Fig. 2.1. In section 2.2.1, we model the transmission dynamics of the seasonal influenza at time t_{m+1}. We keep track of infected individuals during the pandemic influenza since individuals who recover from the pandemic influenza have stronger cross-immunity than those who escaped the pandemic infection. To this end, in section 2.2.2, we model the dynamics of pandemic influenza between the times t_b and t_e. We assume that the distribution of the fraction of susceptible individuals has reached an equilibrium before the pandemic outbreak at time t_b. To find the equilibrium distribution of the fraction of susceptible individuals, in section 2.2.3 we model seasonal influenza epidemics between the time t_1 and $t_m + t_s$ before the pandemic. Knowing all these quantities, we determine if the reproduction number of the seasonal influenza at time t_{m+1} is greater or less than the threshold value of unity, which determines whether or not this seasonal subtype coexists with the pandemic subtype in the season following the pandemic.

We also incorporate vaccination against seasonal influenza to study its influence on subtype coexistence or replacement. We consider two types of vaccine-induced immunity: a temporary one lasting for one year, and a permanent one lasting for life.

In Section 2.3, we present the theoretical and numerical analysis of our model. The model is extended in section 2.4 to incorporate vaccination against seasonal influenza, and a discussion is given in Section 2.5. Our main findings are that the pandemic subtype can replace the previous seasonal subtype at only intermediate levels of cross-immunity, and vaccination at current levels makes replacement only slightly more likely. This appears as a paper: *S. M. Asaduzzaman, Junling Ma, and P. van den Driessche. The coexistence or replacement of two subtypes of influenza. Mathematical Biosciences, 270:1-9, 2015*

2.2 Our Model

The model is a hybrid of ODEs for seasonal influenza before and after the pandemic and the pandemic, with discrete season-to-season mapping.

2.2.1 Invasibility of the Seasonal Influenza After the Pandemic

We model the transmission dynamics of a single seasonal influenza at time t_{m+1} (Fig. 2.1) with a SIR-type model on the fast time scale. The beginning of an epidemic in an ODE-based model is considered as time 0 (corresponding to t_{m+1} on the slow time scale) and its end as time ∞ (corresponding to $t_{m+1}+t_s$ on the slow time scale). At the end of the pandemic, i.e., at time t_e, an individual can be distinguished as either escaped or recovered from the pandemic. Individuals who recovered from the pandemic infection are assumed to have stronger cross-immunity, with these individuals less susceptible to seasonal influenza than those who escaped the pandemic infection. Taking this into account, we assume that each member of the population belongs to one of four classes: susceptible individuals who escaped the pandemic (S), susceptible individuals who recovered from the pandemic ($\widetilde{S}$), infected and infectious individuals (I), and recovered individuals (R). We also use these symbols to represent the fraction of individuals in each class.

Individuals infected and those recovered from a strain of influenza acquire a life long immunity to this strain and a partial cross-immunity to the strains closely related to this strain [30, 42]. The cross-immunity of an individual to the invading strain at t_{m+1} is determined by the individual's infection history. We consider only reduced susceptibility due to this partial cross-immunity. Like Andreasen [4] as given in section 1.5.6, our assumption is that infected individuals acquire the level of cross-immunity (reduced susceptibility) from the last infection, i.e., the level of cross-immunity is only determined by the most recent infection. To reflect the cross-immunity structure of individuals in our model, susceptible individuals are divided into infinitely many sub-classes according to their most recent infection year. We denote by S_0, $\widetilde{S}_0$ the fraction of individuals in S, $\widetilde{S}$ who have never been infected by seasonal subtypes, and by S_i, $\widetilde{S}_i$ for $i \geq 1$ the fraction of individuals in S, $\widetilde{S}$ who were infected i seasons ago. The subscript i denotes the immune status of a susceptible individual. Individuals in S_i, $\widetilde{S}_i$ have susceptibility τ_i, $p\tau_i$ respectively, where τ_i satisfies a monotonic relation $0 < \tau_1 \leq \tau_2 \leq \cdots \leq \tau_n \leq \cdots\cdots \leq \tau_0 = 1$ [30, 61], and $(1-p)$ is the cross-immunity between the pandemic subtype and any seasonal strain. We assume that all individuals

in the population, who were infected by influenza at least once in their lifetime, have the same level of susceptibility p to the pandemic subtype of influenza. This assumption on p is motivated by the fact that influenza viruses share common proteins [77]. For example, H2N2 in 1957 and H3N2 in 1968 are reassortments of other subtypes that were previously circulating in humans [10, 70].

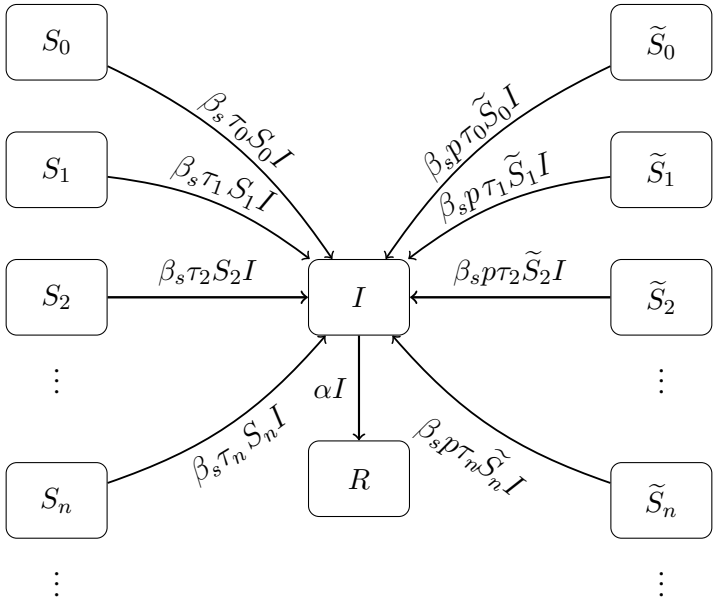

Figure 2.2: The progress of disease dynamics in the $S_i\widetilde{S}_i IR$ model. Here S_i, $\widetilde{S}_i$ are the fraction of individuals with immune status i who escaped, recovered from the pandemic, respectively.

Our model in Fig. 2.2 evolves according to the ODEs

$$\begin{aligned}
\frac{dS_i}{dt} &= -\beta_s\tau_i S_i I \qquad i = 0, 1, 2, \dots , \\
\frac{d\widetilde{S}_i}{dt} &= -\beta_s p\tau_i \widetilde{S}_i I \qquad i = 0, 1, 2, \dots , \\
\frac{dI}{dt} &= \left(\beta_s \sum_{i=0}^{\infty}(\tau_i S_i + p\tau_i \widetilde{S}_i) - \alpha\right) I \, , \\
\frac{dR}{dt} &= \alpha I \, ,
\end{aligned}$$

where α and β_s denote the recovery rate and transmission rate of seasonal influenza. We ignore birth and death processes in the seasonal dynamics, since for influenza the epidemiological time scale is much faster than the demographic time scale, and the number of deaths due to influenza is small. Thus, the total population $\sum_{i=0}^{\infty}(S_i + \widetilde{S}_i) + I + R = 1$ is

a constant. Since the equation for the fraction of recovered individuals is decoupled from the other variables, R can be determined from the other variables, so we do not need to consider the change in the R class. Introduce the non-dimensional time $\hat{t} = t\alpha$, so that the infectious period is 1; the above system of ODEs simplifies to (dropping $\hat{}$)

$$\frac{dS_i}{dt} = -\mathcal{R}_0\tau_i S_i I \qquad i = 0, 1, 2, \dots , \tag{2.1a}$$

$$\frac{d\widetilde{S}_i}{dt} = -\mathcal{R}_0 p\tau_i \widetilde{S}_i I \qquad i = 0, 1, 2, \dots , \tag{2.1b}$$

$$\frac{dI}{dt} = \left(\mathcal{R}_0 \sum_{i=0}^{\infty}(\tau_i S_i + p\tau_i \widetilde{S}_i) - 1\right) I \, , \tag{2.1c}$$

where $\mathcal{R}_0 = \frac{\beta_s}{\alpha}$, the basic reproduction number of seasonal influenza (see section 1.5.1). We assume that at time 0 on the fast time scale, all individuals are susceptible to the seasonal influenza according to their respective immune status i, and a few infectious individuals are introduced into the population. Denote the end of the pandemic influenza as the time t_e (Fig. 2.1). Since there are no recovered individuals at the beginning, the initial conditions for system (2.1) are $S_i(0) = S_i(t_e)$, $\widetilde{S}_i(0) = \widetilde{S}_i(t_e)$ with $\sum_{i=0}^{\infty}\left(S_i(0)+\widetilde{S}_i(0)\right) \approx 1$ and $I(0) = I_0$ positive and small in magnitude, i.e., $I_0 \approx 0$. In our model, from (2.1c), the non-dimensional quantity

$$\mathcal{R}_s = \mathcal{R}_0 \sum_{i=1}^{\infty}(\tau_i S_i(t_e) + p\tau_i \widetilde{S}_i(t_e)) + \mathcal{R}_0(S_0(t_e) + p\widetilde{S}_0(t_e)) \tag{2.2}$$

is the reproduction number that takes into account the cross-immunity of individuals gained from seasonal infections, and the cross-immunity between the pandemic subtype and the $(m+1)$st seasonal strain. This number determines a threshold. If $\mathcal{R}_s > 1$, then a seasonal epidemic occurs, i.e., the seasonal subtype coexists with the pandemic subtype in the season following the pandemic, and if $\mathcal{R}_s < 1$, then the seasonal subtype is replaced by the pandemic subtype [31].

2.2.2 Dynamics of Pandemic Influenza

Because the quantity $\mathcal{R}_s$ in (2.2) depends on $S_i(t_e)$, $\widetilde{S}_i(t_e)$, we now model the transmission dynamics of pandemic influenza from t_b to t_e (Fig. 2.1), which corresponds to time zero and time infinity on the fast time scale, to indicate the beginning and the end of the pandemic outbreak. At the beginning of the pandemic influenza, there are no $\widetilde{S}_i$ classes. However,

there are S_i classes with the meaning in section 2.2.1. We assume that the fraction of susceptible individuals in S_i has reached an equilibrium distribution S_i^*, for $i \geq 0$, before a pandemic subtype causes an outbreak. As assumed in section 2.2.1, the individuals in S_0^* have susceptibility 1 to the pandemic subtype, since these individuals have never been infected by seasonal influenza, and $(1-p)$ is the cross-immunity between the pandemic subtype and any seasonal strain. Our pandemic influenza model is

$$\frac{dS_0}{dt} = -\mathcal{R}_{0_p} S_0 I \,, \tag{2.3a}$$

$$\frac{dS_i}{dt} = -\mathcal{R}_{0_p} p S_i I \qquad i = 1, 2, \ldots \,, \tag{2.3b}$$

$$\frac{dI}{dt} = \big(\mathcal{R}_{0_p}(\sum_{i=1}^{\infty} p S_i + S_0) - 1\big) I \,, \tag{2.3c}$$

$$\lambda_p = \mathcal{R}_{0_p} I \,, \tag{2.3d}$$

with initial conditions $S_i(0) = S_i^*, I(0) = I_0 > 0$ with $\sum_{i=0}^{\infty} S_i^* \approx 1$. Here, $\mathcal{R}_{0_p}$ is the basic reproduction number of the pandemic influenza in a completely susceptible population, and λ_p is the force of infection on individuals to the pandemic subtype of influenza. We ignore demographics for the same reason as in section 2.2.1, and also ignore death due to the pandemic because the case fatality rate of the pandemic influenza in 1918 was about 2% to 2.5% and it was less than 0.1% for other pandemics in the last century [72]. From (2.3c), the reproduction number of the pandemic influenza, taking cross-immunity into account, is given by the non-dimensional quantity

$$\mathcal{R}_p = \mathcal{R}_{0_p}(p(1 - S_0^*) + S_0^*) \,. \tag{2.4}$$

If $\mathcal{R}_p < 1$, then no pandemic occurs; whereas if $\mathcal{R}_p > 1$, then there is a pandemic [31]. Note that, if S_0^* is negligible, then $\mathcal{R}_p \approx p\mathcal{R}_{0_p}$. We now calculate analytically the final state of the pandemic influenza by observing from (2.3a) and (2.3b) that

$$\frac{dS_i}{dS_0} = \frac{pS_i}{S_0}, \quad i = 1, 2, \ldots \,.$$

Integrating the above equations from time t_b (0 on the fast time scale) to t gives

$$S_i(t) = S_i(0)\left(\frac{S_0(t)}{S_0(0)}\right)^p, \quad i = 1, 2, \ldots \,. \tag{2.5}$$

At the end of the pandemic, i.e., at time t_e (∞ on the fast time scale), the fraction of susceptibles who have never been infected by the seasonal influenza and escaped the pandemic infection is denoted by $\psi = \frac{S_0(\infty)}{S_0^*}$. Then the final size equations at $t = t_e$ ($t = \infty$ on the fast time scale) are given by

$$\begin{aligned} S_0(\infty) &= \psi S_0^*\,, & \widetilde{S}_0(\infty) &= S_0^*(1-\psi) \\ S_i(\infty) &= \psi^p S_i^*\,, & \widetilde{S}_i(\infty) &= S_i^*(1-\psi^p) \qquad i = 1, 2, \dots\,, \end{aligned}$$

which relate the final state of the pandemic for individuals with immune status i to seasonal influenza in terms of the fraction of susceptibles at the beginning of the pandemic and the fraction of individuals who have never been infected by the seasonal influenza.

Using (2.5), the derivative of the force of infection λ_p in (2.3d) can be written in the following form

$$\frac{d\lambda_p}{dS_0} = \frac{1}{S_0(t)} - \frac{p\mathcal{R}_{0_p}}{S_0(t)} \sum_{i=1}^{\infty} S_i(0) \left(\frac{S_0(t)}{S_0(0)} \right)^p - \mathcal{R}_{0_p}$$

with solution

$$\lambda_p(t) - \lambda_p(0) = \log\left(\frac{S_0(t)}{S_0(0)} \right) - \mathcal{R}_{0_p} \sum_{i=1}^{\infty} S_i(0) \left[\left(\frac{S_0(t)}{S_0(0)} \right)^p - 1 \right] - \mathcal{R}_{0_p} \big(S_0(t) - S_0(0) \big)\,.$$

The force of infection $\lambda_p(0)$ at the beginning of the pandemic is very small since only a few infectious individuals are introduced into the population, so it can be taken as zero. When the pandemic is over at $t = \infty$, the force of infection is also zero because no one is infectious anymore. Thus at $t = \infty$, ψ must satisfy the implicit equation

$$\log(\psi) = \mathcal{R}_{0_p} \big[\psi^p (1 - S_0^*) + S_0^* \psi - 1 \big]\,. \tag{2.6}$$

The equation (2.6) has a unique root $\psi \in (0, 1)$ if $\mathcal{R}_p > 1$. To show that (2.6) has a unique root $\psi \in (0, 1)$, consider

$$h(\psi) = \log(\psi) - \mathcal{R}_{0_p} \big[\psi^p (1 - S_0^*) + S_0^* \psi - 1 \big].$$

Then $h(1) = 0$ and $\lim_{\psi \to 0^+} h(\psi) = -\infty$, and

$$h'(\psi) = \frac{1}{\psi} \big[1 - \mathcal{R}_{0_p} \big(p\psi^p (1 - S_0^*) + \psi S_0^* \big) \big], \tag{2.7}$$

which gives $h'(1) = 1 - \mathcal{R}_{0_p}\big(p(1 - S_0^*) + S_0^*\big) = 1 - \mathcal{R}_p$. Thus (2.6) has at least one root $\psi \in (0, 1)$ if $h'(1) < 0$, i.e., $\mathcal{R}_p > 1$. Now consider

$$g(\psi) = 1 - \mathcal{R}_{0_p}\big(p\psi^p(1 - S_0^*) + \psi S_0^*\big)\,.$$

Then, $\lim_{\psi\to 0^+} g(\psi) = 1$ and $g(1) = 1 - \mathcal{R}_p < 0$ if $\mathcal{R}_p > 1$. The term $\mathcal{R}_{0_p}\big(p\psi^p(1 - S_0^*) + \psi S_0^*\big)$ is a monotonic increasing function for $\psi \in (0, 1)$. Thus $g(\psi)$ has a unique root $\bar{\psi} \in (0, 1)$, which implies that $h(\psi)$ has a unique critical point $\bar{\psi} \in (0, 1)$. Thus, $h(\psi)$ is concave down for $\psi \in (0, 1)$, which completes the proof of the uniqueness of $\psi \in (0, 1)$.

Using the values of $S_0(\infty)$ and $S_i(\infty)$, the attack rate Z of the pandemic influenza is given by

$$\begin{aligned} Z &= 1 - \big(S_0(\infty) + \sum_{i=1}^{\infty} S_i(\infty)\big) \\ Z &= 1 - \big(\psi S_0^* + \psi^p(1 - S_0^*)\big). \end{aligned} \tag{2.8}$$

Note that we found the attack rate $Z = 1 - \psi$ with $\psi = \frac{S(\infty)}{S(0)}$ in section 1.5.1, for a simple SIR-type model that does not distinguish between the susceptibility of individuals. The simple SIR-type model assumes that all the individuals have susceptibility 1; whereas the pandemic model in (2.3) assumes a varying susceptibility for individuals. The basic reproduction number of seasonal influenza in (2.2) can be written as

$$\mathcal{R}_s = \mathcal{R}_0 \sum_{i=1}^{\infty} \tau_i S_i^*(\psi^p + p(1 - \psi^p)) + \mathcal{R}_0 S_0^*(\psi + p(1 - \psi))\,. \tag{2.9}$$

2.2.3 Dynamics of Seasonal Influenza Before the Pandemic

In order to determine all S_i^* in (2.9), we model the dynamics of seasonal influenza in the m seasons between the time t_1 and $t_m + t_s$ based on the annual structure of Andreasen's [4] seasonal model as given in section 1.5.6. This dynamics is influenced by the dynamics of a single season.

The Dynamics of Single Season Epidemics

As assumed in section 2.2.1, we take time t_k on the slow time scale as time 0 when a seasonal epidemic begins, and time $t_k + t_s$ on the slow time scale as time ∞ when the epidemic is over. Unlike Andreasen [4] as given in section 1.5.6, we do not assume

that cross-immunity lasts only for a finite number of seasons. Also, we do not consider infectivity (σ_i) of individuals in the seasonal model. Following the assumptions in section 2.2.1 without $\widetilde{S}_i$, our one season influenza epidemic model is

$$\begin{aligned} \frac{dS_i}{dt} &= -\mathcal{R}_0\tau_i S_i I \qquad i = 0, 1, 2, \dots , && \text{(2.10a)} \\ \frac{dI}{dt} &= \big(\mathcal{R}_0 \sum_{i=0}^{\infty} \tau_i S_i - 1\big) I \, , && \text{(2.10b)} \\ \lambda_s &= \mathcal{R}_0 I \, , && \text{(2.10c)} \end{aligned}$$

with initial conditions $S_i(0) \geq 0$ with $\sum_{i=0}^{\infty} S_i(0) \approx 1$ and $I(0) = I_0 > 0$. Here, λ_s is the force of infection on individuals to the seasonal strain of influenza. From (2.10b), the reproduction number of seasonal influenza, taking cross-immunity into account, is given by the quantity

$$\mathcal{R} = \mathcal{R}_0 \sum_{i=0}^{\infty} \tau_i S_i(0) \, . \tag{2.11}$$

If $\mathcal{R} > 1$, then a seasonal epidemic occurs and if $\mathcal{R} < 1$, then there is no seasonal epidemic [31]. Following the calculations as in section 2.2.2, when the seasonal epidemic is over the final state of this seasonal epidemic is determined by the equations

$$\begin{aligned} \log(\phi) &= \mathcal{R}_0 \sum_{i=0}^{\infty} S_i(0)\big(\phi^{\tau_i} - 1\big) \, , && \text{(2.12a)} \\ S_i(\infty) &= \phi^{\tau_i} S_i(0), \qquad i = 0, 1, 2, \dots , && \text{(2.12b)} \end{aligned}$$

where ϕ denote the fraction of susceptible individuals who have never been infected by the seasonal influenza and escaped seasonal influenza in the current season, i.e., $\phi = \frac{S_0(\infty)}{S_0(0)}$. If $\mathcal{R} > 1$, then (2.12a) uniquely determines the value of ϕ. Analytically, the uniqueness of ϕ can be proved with a similar argument as for the uniqueness of ψ in section 2.2.2. Thus, for given $\tau_i, \mathcal{R}_0$ and $S_i(0)$, the fraction of susceptible individuals with immune status i who escaped influenza in the current season can be found by solving ϕ from (2.12a) and using ϕ in (2.12b).

Season-to-Season Mapping

We found the final state of a seasonal epidemic and determined how the immune status of individuals changes in the seasonal dynamics of influenza. We now want to determine how the immune status of individuals changes from the onset of one epidemic season

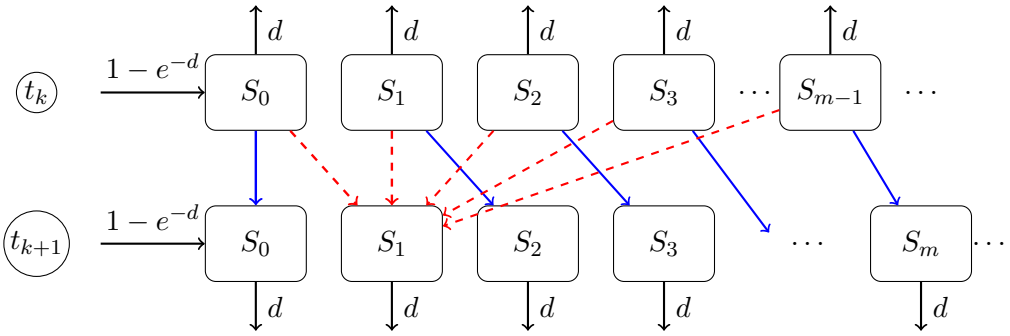

Figure 2.3: The change of immune status of the fraction of susceptible individuals from the end of the t_k season to the beginning of the t_{k+1} season. The change of immune status of the individuals who escaped infection is shown as a solid line and for those who recovered from the infection is shown as a dashed line. Vertical arrows show natural death at a rate d from each S_i class and horizontal arrows show birth at a rate $(1-e^{-d})$ to the S_0 class.

to the beginning of the next epidemic season. We ignored demographics in the seasonal dynamics of influenza on the fast time scale because the number of births and deaths in a single season is negligible, but for a long time horizon, demographic events may have a significant effect on the dynamics of influenza. On the slow time scale, we now incorporate demographics in the dynamics of influenza by including newborn individuals into the S_0 class, since newborn individuals are completely susceptible. We assume that an individual's life expectancy is exponentially distributed with parameter d, thus the survival probability of an individual is e^{-d}.

At the beginning of the t_k season, $S_i(t_k)$ for $i \geq 1$ denotes the fraction of susceptible individuals with immune status i and ϕ denotes the fraction of individuals who have never been infected by seasonal influenza and escaped infection during the t_k season; see Fig. 2.1 for time line. The individuals with immune status i who escaped influenza during the t_k season acquire immune status $(i+1)$ at the beginning of the t_{k+1} season because then their most recent infection is $(i+1)$ seasons old; see Fig. 2.3. Thus the fraction of susceptible individuals at the beginning of the t_{k+1} season is

$$S_{i+1}(t_{k+1}) = \phi^{\tau_i} S_i(t_k) e^{-d} \qquad i = 1, 2, \ldots , \tag{2.13}$$

where ϕ in season t_k is a solution in $(0,1)$ of (2.12a).

At the beginning of the t_{k+1} season, the fraction of susceptible individuals in the S_1 class is determined by the fact that the individuals from all S_i classes who were infected

during the t_k season have received a booster by the infection. These individuals have one year old immune status at the beginning of the t_{k+1} season; see Fig. 2.3. Thus,

$$S_1(t_{k+1}) = \big(1 - \sum_{i=0}^{\infty} \phi^{\tau_i} S_i(t_k)\big) e^{-d} \,. \tag{2.14}$$

At the beginning of the t_k season, $S_0(t_k)$ denotes the fraction of susceptible individuals who have never been infected. The individuals in the S_0 class who escaped influenza during the t_k season remain in the S_0 class with the newborn individuals; see Fig. 2.3. Thus,

$$S_0(t_{k+1}) = \phi S_0(t_k) e^{-d} + (1 - e^{-d}) \,. \tag{2.15}$$

The season-to-season mapping that determines the change of immune status is given by (2.13)-(2.15); see also [4, Eqs.(9)-(10)]. The equilibrium distribution of the fraction of susceptible individuals S_i^*, is found by solving the mapping equations (2.13)-(2.15). In section 2.2.2, we assumed that this fraction has reached an equilibrium before the pandemic arrives. The reproduction number of seasonal influenza at equilibrium, from (2.11) is given by

$$\mathcal{R}^* = \mathcal{R}_0 \sum_{i=0}^{\infty} \tau_i S_i^* \,. \tag{2.16}$$

2.3 Results

We first find a theoretical threshold condition on p for an outbreak of pandemic influenza, and if there is such an outbreak, we use numerical simulations to predict whether or not a seasonal subtype survives in the season following a pandemic.

2.3.1 Theoretical Results

For a given value of p and $\mathcal{R}_{0_p}$, (2.6) can be solved to find ψ, the fraction of individuals who have never been infected by the seasonal influenza and escaped the pandemic infection. Equation (2.6) always has a root at $\psi = 1$, which is not biologically interesting, since $\psi = 1$ means there is no pandemic, and (2.6) cannot have a root at $\psi = 0$ as the equation is not defined at $\psi = 0$. The uniqueness of $\psi \in (0, 1)$ if $\mathcal{R}_p > 1$ gives $p > \frac{\frac{1}{\mathcal{R}_{0_p}} - S_0^*}{1 - S_0^*}$ (from $h'(1) < 0$, section 2.2.2), which imposes a lower bound on p, the susceptibility to the pandemic subtype of influenza, for an outbreak.

The reproduction number $\mathcal{R}_s$ of seasonal influenza after the pandemic given in (2.9), is a non-linear function of $\mathcal{R}_0$, $\mathcal{R}_{0_p}$, p and ψ from (2.6). At the upper extreme $p = 1$, from (2.9) the value of $\mathcal{R}_s = \mathcal{R}_0 \sum_{i=1}^{\infty} \tau_i S_i^* + \mathcal{R}_0 S_0^*$, which equals $\mathcal{R}^*$ in (2.16). At the lower extreme $p = 0$, from (2.9) the value of $\mathcal{R}_s = \mathcal{R}_0 \sum_{i=1}^{\infty} \tau_i S_i^* + \mathcal{R}_0 S_0^* \hat{\psi}$, where $\hat{\psi}$ satisfies (2.6) with $p = 0$, i.e., $\log(\hat{\psi}) = \mathcal{R}_{0_p} S_0^* (\hat{\psi} - 1)$. This equation has a root $\hat{\psi} \in (0, 1)$ if $\mathcal{R}_{0_p} S_0^* > 1$. Thus the reproduction number $\mathcal{R}_s$ of the seasonal influenza at the lower extreme $p = 0$ is less than $\mathcal{R}^*$ if $\mathcal{R}_{0_p} S_0^* > 1$; whereas $\mathcal{R}_s$ is equal to $\mathcal{R}^*$ if $\mathcal{R}_{0_p} S_0^* < 1$, since (2.6) with $p = 0$ has only the root $\hat{\psi} = 1$.

Differentiating (2.6) with respect to $\mathcal{R}_{0_p}$, $\frac{\partial \psi}{\partial \mathcal{R}_{0_p}} = \frac{S_0^*(\psi - \psi^p) + (\psi^p - 1)}{h'(\psi)}$, where $h'(\psi)$ is given in (2.7). If there is a pandemic outbreak, then $\psi \in (0, \bar{\psi})$; thus $h'(\psi) > 0$ on this interval. Biologically, $h'(\psi)$ is some positive constant multiple of one minus the reproduction number of the pandemic subtype at time infinity. The reproduction number of the pandemic subtype at the end of the pandemic is smaller than unity, since the pandemic has come to an end. The numerator of $\frac{\partial \psi}{\partial \mathcal{R}_{0_p}}$ is negative for any $\psi \in (0, 1)$ giving $\frac{\partial \psi}{\partial \mathcal{R}_{0_p}} < 0$. Thus ψ decreases with increasing $\mathcal{R}_{0_p}$. From (2.9), $\frac{\partial \mathcal{R}_s}{\partial \psi} = (1 - p)\big[p\psi^{p-1}\mathcal{R}_0 \sum_{i=1}^{\infty} \tau_i S_i^* + \mathcal{R}_0 S_0^*\big] > 0$, i.e., $\mathcal{R}_s$ increases with increasing ψ. These relations give $\frac{\partial \mathcal{R}_s}{\partial \mathcal{R}_{0_p}} < 0$, which indicates that the reproduction number of seasonal influenza after the pandemic decreases with increasing basic reproduction number $\mathcal{R}_{0_p}$ of the pandemic subtype.

2.3.2 Simulation Results

Assuming that the basic reproduction number $\mathcal{R}_0$ in a completely susceptible population and the cross-immunity structure τ_i do not change from season to season, (2.13)-(2.15) describe a discrete dynamical system giving the season-to-season dynamics of influenza epidemics. The susceptibility τ_i is taken equal to $(1 - q^i), 0 \leq q \leq 1$. Here q is the probability of antibodies from the previous year's strain binding to the current seasonal strain of influenza. This assumption satisfies the monotonic relation stated in section 2.2.1. For the simulations, we take $q = 0.75$, estimated from [22], except in Fig. 2.5 where we take a range of q values.

In our simulations, we take a large number (m) of immune classes of susceptible individuals. For sufficiently large m, $\tau_m \approx \tau_{m+1}$, i.e., the susceptibility of individuals in immune class S_m is almost equal to that in immune class S_{m+1}. Thus, individuals in the immune class S_m who escaped influenza infection during the t_k season remain in the same class at the beginning of the t_{k+1} season.

We numerically simulated the model to understand the seasonal dynamics of influenza

epidemics on the long time scale and to find the equilibrium distribution of susceptible individuals, S_i^*. For the parameter values used in these simulations, the convergence to S_i^* is attained in 10 – 12 seasons, thus validating our assumption that $S_i(t)$ approaches S_i^* before the pandemic arrives. Our numerical simulations started with an initial guess of susceptible individuals $S_i(0)$ such that $\sum_{i=0}^{m} S_i(0) \approx 1$. Using this initial guess of $S_i(0)$, and a value of $\mathcal{R}_0$, the fraction of susceptible individuals ϕ who have never been infected by seasonal influenza and escaped infection in the current season was determined by solving (2.12a). The final state of the epidemic was found from (2.12b). For illustration, we take $d = 0.0124$, which corresponds to the life expectancy of 80.7 years in the Canadian population in 2010 [45]. The immune status of individuals at the beginning of the next season was determined by using the season-to-season mapping equations (2.13)-(2.15). The new susceptible values were then used as initial values and the cycle recomputed. This process continued until the equilibrium distribution of susceptible individuals S_i^* was achieved. We found that for $i = 1, \ldots, m$, the equilibrium value of S_i exists in $[0, 1]$, and is unique. For our choice of parameters and assumption that infectivity is not reduced by cross-immunity, we found no sustained oscillations for $S_i(t)$ (cf. [4]).

We used the values of S_i^* as initial susceptibles at the beginning of the pandemic influenza. For a given p, S_0^* and $\mathcal{R}_{0_p}$, ψ was found by solving (2.6). The reproduction number $\mathcal{R}_s$ of seasonal influenza after the pandemic was then computed from (2.9). Fig. 2.4 is a plot of the reproduction number $\mathcal{R}_s$ of seasonal influenza after the pandemic against p. These plots show that for small values of p, i.e., for very high cross-immunity $(1-p)$, there is no outbreak of pandemic influenza (Fig. 2.4, horizontal part in each plot). Numerical simulations agree with the theoretical condition found in section 2.3.1 for a pandemic outbreak, i.e., the pandemic subtype of influenza cannot cause an outbreak if $p < \frac{\frac{1}{\mathcal{R}_{0_p}} - S_0^*}{1 - S_0^*}$. If there is an outbreak of pandemic influenza, the pandemic subtype coexists with the seasonal subtype if $\mathcal{R}_s > 1$ (Fig. 2.4, range of p values for which $\mathcal{R}_s > 1$). If $\mathcal{R}_{s_{\text{min}}} < 1$, then the range of values of p was found numerically (Fig. 2.4, range of p values for which $\mathcal{R}_s < 1$), with the pandemic subtype replacing the seasonal subtype when p belongs to this range. The replacement of the seasonal subtype by the pandemic subtype becomes easier when the basic reproduction number $\mathcal{R}_{0_p}$ of the pandemic subtype increases (Fig. 2.4, left to right in each row); the range for pandemic influenza to replace seasonal influenza decreases as the basic reproduction number $\mathcal{R}_0$ of seasonal influenza increases (Fig. 2.4, top to bottom in each column).

Fig. 2.5 is a plot of the reproduction number $\mathcal{R}_s$ of seasonal influenza against p for different susceptibility $\tau_i = (1 - q^i)$ to the seasonal influenza. The replacement of the

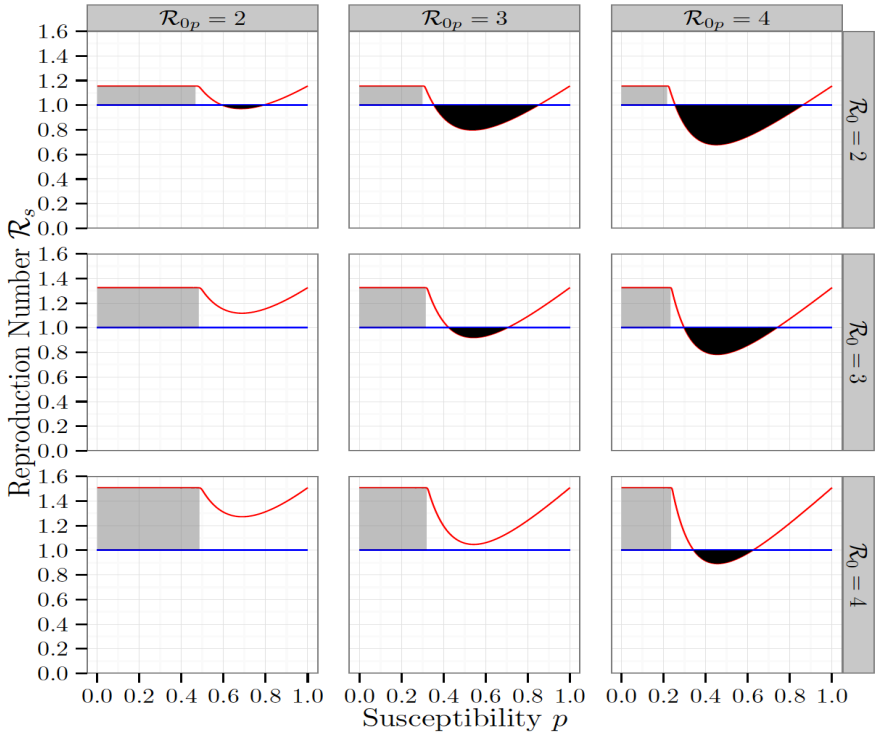

Figure 2.4: The curves $\mathcal{R}_s$ plotted as a function of p, giving the range of p values for which the seasonal subtype is replaced by the pandemic subtype or reappears after the pandemic. $\mathcal{R}_0$ and $\mathcal{R}_{0_p}$ represent the basic reproduction number of seasonal influenza and pandemic influenza, respectively. The pandemic subtype of influenza cannot invade in the rectangular region (light shaded) for small p values but replaces the seasonal subtype (dark shaded) and coexists with the seasonal subtype in the season following the pandemic (not shaded) above $\mathcal{R}_s = 1$ (marked by a horizontal line). Note that each plot shown has $q = 0.75$ and $\mathcal{R}_{0_p} S_0^* < 1$.

seasonal subtype by the pandemic subtype becomes easier as the susceptibility to the seasonal influenza decreases (Fig. 2.5, top to bottom), i.e., with increasing q, the probability of antibodies from the previous year's strain binding to the current seasonal strain of influenza.

2.4 Vaccination Against Seasonal Influenza

We extend our seasonal model of section 2.2.3 to incorporate vaccination against seasonal influenza. Given the normal practice for vaccination, we assume that vaccines are administered before the start of the seasonal epidemic. For simplicity of our model, we ignore any age-specific effects of vaccination. Our assumption is that the effective

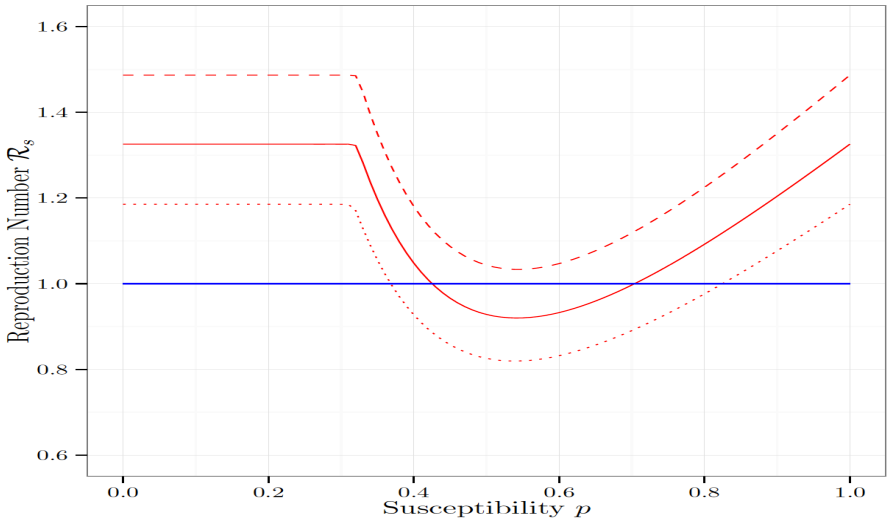

Figure 2.5: As Fig. 2.4 with parameters $\mathcal{R}_0 = 3$, $\mathcal{R}_{0_p} = 3$ and $\tau_i = (1 - q^i)$ but varying $q = 0.65$ (dashed curve), 0.75 (solid curve) and 0.85 (dotted curve), respectively.

vaccination coverage ϵ (vaccine effectiveness times vaccine coverage), which has been achieved before the beginning of the seasonal influenza epidemic, reduces the available fraction of susceptibles by a factor ϵ. We assume that the duration of vaccine-induced immunity lasts for one year (section 2.4.1), or for life (section 2.4.2).

2.4.1 Vaccination Gives Immunity for One Year

We assume here that the effectiveness of vaccination lasts for one year, i.e., vaccinated individuals are protected from influenza infection for the season in which they are vaccinated. The immune status i of vaccinated individuals at the beginning of the next season is the same as those of unvaccinated individuals who escaped influenza infection during the season (Fig. 2.6). Thus, one year effective vaccine works as if the individuals naturally escaped the influenza infection. The transmission dynamics of our seasonal model is not changed; but is now applied to the unvaccinated individuals. The season-to-season dynamics of influenza is as follows:

$$S_{i+1}(t_{k+1}) = (1-\epsilon)S_i(t_k)\phi^{\tau_i}e^{-d} + \epsilon S_i(t_k)e^{-d} \qquad i = 1, 2, \dots, \tag{2.17a}$$

$$S_1(t_{k+1}) = (1-\epsilon)\big(1 - \sum_{i=0}^{\infty} S_i(t_k)\phi^{\tau_i}\big)e^{-d}, \tag{2.17b}$$

$$S_0(t_{k+1}) = (1-\epsilon)S_0(t_k)\phi e^{-d} + \epsilon S_0(t_k)e^{-d} + (1 - e^{-d}), \tag{2.17c}$$

We numerically simulated the model (2.17) to find the susceptible fraction S_i^* at

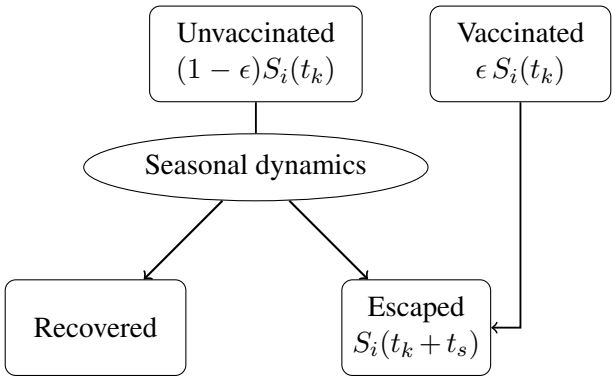

Figure 2.6: The flow diagram of individuals during the seasonal epidemic when the effectiveness of vaccination lasts for one year and effective vaccination fraction is ϵ.

equilibrium. The reproduction number $\mathcal{R}_s$ of seasonal influenza after the pandemic is given by

$$\mathcal{R}_s = (1-\epsilon)\mathcal{R}_0 \sum_{i=1}^{\infty} \tau_i S_i^*(\psi^p + p(1-\psi^p)) + (1-\epsilon)\mathcal{R}_0 S_0^*(\psi + p(1-\psi))\,. \qquad (2.18)$$

From data influenza vaccine has an overall effectiveness of 60% [74] and the current seasonal influenza vaccine coverage in Canada ranges between 25%–41% across ethnic groups [63]. Following these we choose $\epsilon = 0.15$ and 0.24 corresponding to 15% and 24% effective vaccination coverage of the total population. We also choose $\epsilon = 0.60$ corresponding to 100% coverage of vaccination in the population with the present effectiveness of vaccine. These plots in Fig. 2.7 of $\mathcal{R}_s$ from (2.18) show that as vaccination against seasonal influenza increases, the range of p values for the pandemic subtype to replace the seasonal subtype increases but with the current vaccine coverage $(25\%$–$41\%)$ this increase is slight (compare with Fig. 2.4). However, if vaccine coverage of 100% is achieved, then the range of p values for the pandemic subtype to replace the seasonal subtype increases significantly, e.g., for $\mathcal{R}_{0_p} = 3$ and $\mathcal{R}_0 = 4$, the pandemic subtype replaces the seasonal subtype, whereas at the current vaccine coverage the pandemic subtype cannot replace the seasonal subtype. Also if $\mathcal{R}_0 = 2$, then 100% vaccine coverage prevents a seasonal epidemic.

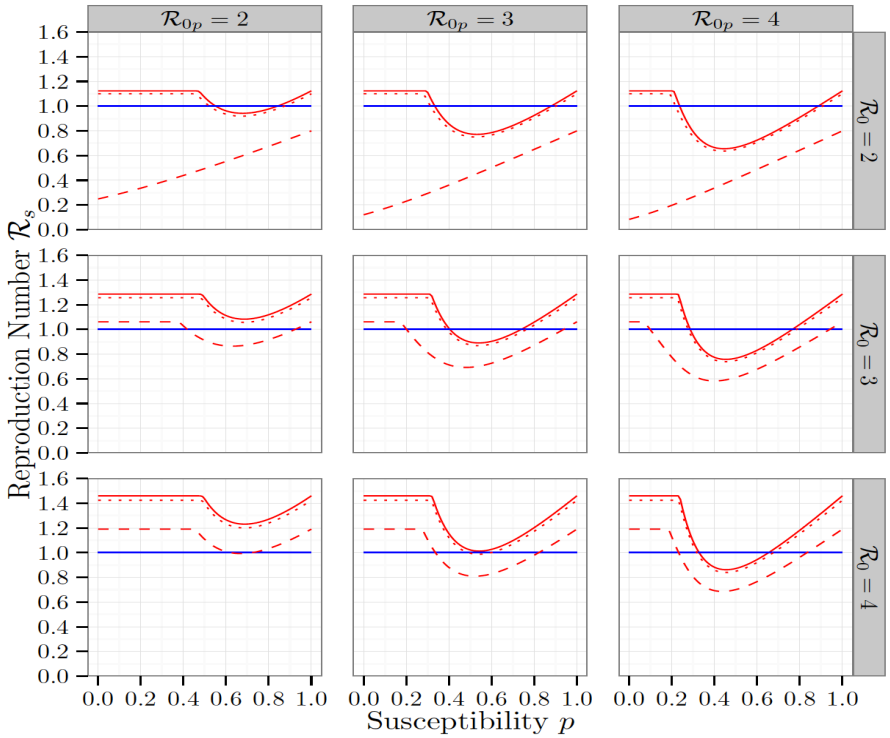

Figure 2.7: As Fig. 2.4, but with vaccination giving immunity for one year. Vaccine efficacy in preventing seasonal influenza infection is 60% and effective vaccination coverage is 15% (solid line), 24% (dotted line) and 60% (dashed line). Compare with Fig. 2.4 (no vaccination).

2.4.2 Vaccination Gives Lifetime Immunity

Empirical studies [22, 39]) found that the effectiveness of vaccination lasts for more than one year. We assume that the effectiveness of vaccination lasts for many years, i.e., vaccinated individuals are protected from influenza infection for life (Fig. 2.8). We assume that the duration and protection efficacy of naturally-acquired immunity and vaccine-induced immunity are the same for the subsequent seasonal epidemic. When vaccine gives the lifetime immunity, vaccination is working as if the vaccinated individuals have recovered from influenza infection. The season-to-season dynamics of influenza is as follows:

$$S_{i+1}(t_{k+1}) = (1-\epsilon)S_i(t_k)\phi^{\tau_i}e^{-d} \qquad i = 1, 2, \dots, \tag{2.19a}$$

$$S_1(t_{k+1}) = (1-\epsilon)\big(1 - \sum_{i=0}^{\infty} S_i(t_k)\phi^{\tau_i}\big)e^{-d} + \epsilon \sum_{i=1}^{\infty} S_i(t_k)e^{-d}\,, \tag{2.19b}$$

$$S_0(t_{k+1}) = (1-\epsilon)S_0(t_k)\phi e^{-d} + \epsilon S_0(t_k)e^{-d} + (1-e^{-d})\,. \tag{2.19c}$$

Fig. 2.9 is a plot of the reproduction number $\mathcal{R}_s$ from (2.18) (with different S_i^*) of seasonal

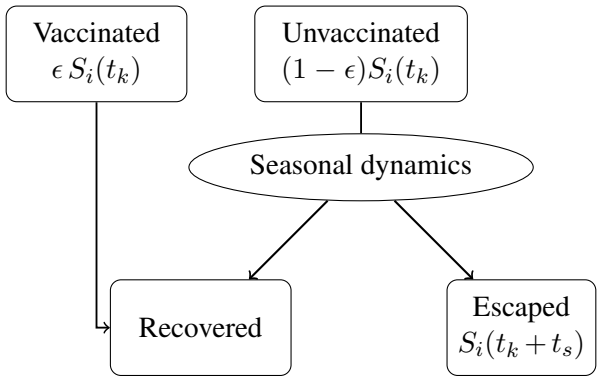

Figure 2.8: The flow diagram of individuals during the seasonal epidemic when the effectiveness of vaccine gives lifetime immunity and the effective vaccination fraction is ϵ.

influenza after the pandemic against p values for different values of $\mathcal{R}_0$ and $\mathcal{R}_{0_p}$. As in section 2.4.1, we choose $\epsilon = 0.15, 0.24$ and 0.60 corresponding to 15%, 24% and 60% effective vaccination coverage of the total population. The qualitative behavior of these plots (Fig. 2.9) is the same as those for the model when vaccine-induced immunity lasts for one year (Fig. 2.7). However, the range of p values for the pandemic subtype to replace the seasonal subtype increases with longer vaccine induced immunity.

2.5 Discussion

We have developed a hybrid model for studying the interaction between an influenza A pandemic subtype and a seasonal subtype with several strains. During a seasonal epidemic or pandemic, time is taken as continuous giving a system of ODEs; whereas for the season-to-season mapping, time is discrete. Seasonal epidemics are modeled by a modification of Andreasen's system [4], which assumes that the cross-immunity of an individual to the challenging seasonal strain is determined by the last season that an individual was infected. Based on the observation that pandemics and seasonal epidemics do not overlap in time, the pandemic is assumed to occur between two seasonal epidemics, with the infection history distribution having reached equilibrium before the pandemic starts. Cross-immunity between the seasonal subtype and the pandemic subtype is assumed to be independent of the infection history for the seasonal strains.

We found that a larger basic reproduction number $\mathcal{R}_0$ for the seasonal subtype makes it harder for the pandemic to replace the seasonal one. In fact, a larger seasonal basic

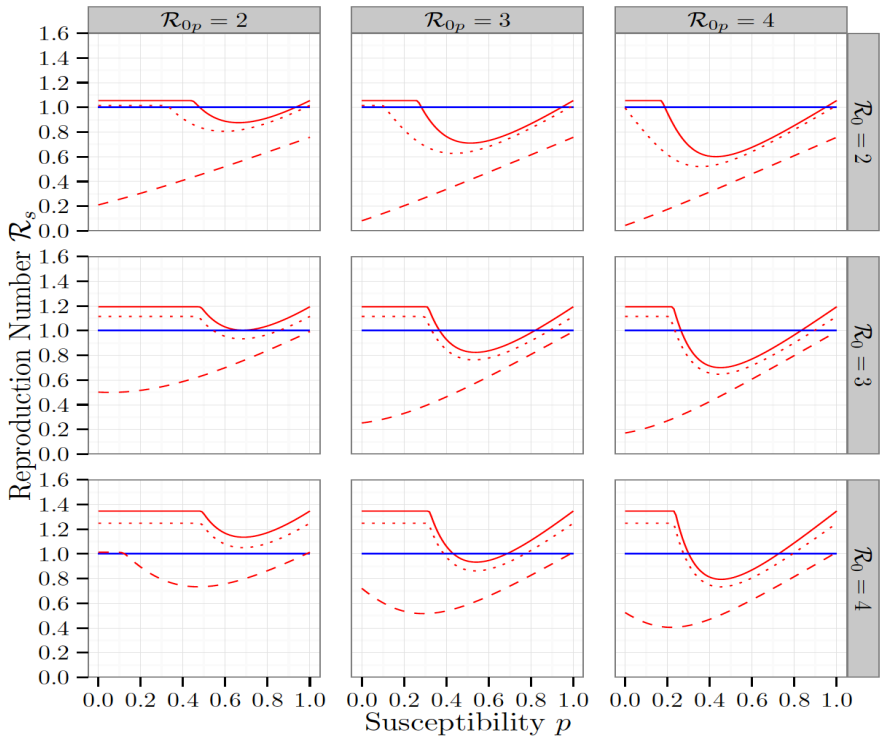

Figure 2.9: As Fig. 2.7, except that vaccination gives lifetime immunity.

reproduction number increases the equilibrium seasonal reproduction number $\mathcal{R}^*$, but does not effect the population level cross-immunity caused by the pandemic to the seasonal strain after the pandemic. Thus the seasonal reproduction number $\mathcal{R}_s$ after the pandemic increases. On the other hand, a larger basic reproduction number $\mathcal{R}_{0_p}$ for the pandemic makes replacement easier. Intuitively, a larger pandemic basic reproduction number increases the fraction infected by the pandemic, and thus increases the population level cross-immunity to the seasonal strain after the pandemic.

Our model and results are given in terms of p, which is the susceptibility of individuals to the pandemic subtype, but it is instructive to interpret the results in terms of the cross-immunity $(1 - p)$ between the seasonal and pandemic subtype. Very strong cross-immunity between the pandemic and the seasonal subtype prevents the invasion of the pandemic, because the pandemic reproduction number is reduced below unity. As $(1 - p)$ decreases, the pandemic may occur, but does not confer a large enough population level cross-immunity to prevent the invasion of the next seasonal epidemic, causing the pandemic and seasonal subtypes to coexist in the season following the pandemic. As cross-immunity decreases further, the pandemic increases, and eventually may cause large enough population cross-immunity to prevent the next seasonal strain invading. If this

occurs, the pandemic replaces the seasonal strain. However, as $(1-p)$ decreases close to zero, the pandemic and the seasonal subtypes become essentially independent; thus, small cross-immunity causes the pandemic and seasonal subtype to coexist. This means that the pandemic may replace the seasonal subtype for only intermediate levels of cross-immunity.

We considered vaccination against seasonal influenza, as this is currently available in Canada and many other countries; however, we have not considered vaccination against the pandemic subtype, as a vaccine is unlikely to be produced early enough to give significant reduction of the pandemic. We found that vaccination reduces seasonal reproduction numbers, and thus replacement by the pandemic subtype occurs more easily. However, for current levels of vaccine coverage and efficacy in Canada, this reduction is negligible. With the current vaccine efficacy of 60%, if vaccination uptake could be raised to 100%, then reduction of the seasonal reproduction number is significant and the pandemic subtype is more likely to replace the seasonal subtype.

Chapter 3

Estimation of cross-immunity between drifted strains of influenza A/H3N2

3.1 Introduction

Seasonal influenza A strains tend to group in antigenic clusters rather than form a continuous antigenic lineage [69]. Usually the strains in a cluster have small antigenic distance (number of different epitopes), and remain dominant for 3.3 seasons on average before a new cluster at a larger antigenic distance emerges [69]. This makes it very difficult to predict which strains are going to cause an outbreak in the next season. Influenza vaccine is a main strategy for prevention and control of seasonal and pandemic influenza [27, 34]. The usual practice is that influenza vaccines are administered before the start of the seasonal epidemic. Due to antigenic drift, influenza vaccines (that are derived from the strains in the past season) are not completely protective in the next season against infection by drifted strains. However, influenza vaccine and natural infection give rise to cross-immunity (see section 1.5.4) [62, 80]. Cross-immunity has a major influence on the final size (the fraction of individuals infected in an influenza outbreak, also called the attack rate) of seasonal epidemics [4, 5]. Thus cross-immunity also influences the distribution of susceptibility in the population, which in turn shapes the natural selection of influenza strains [37]. In addition, cross-immunity between the vaccine and challenging strains is a crucial measure for vaccine protection.

In chapter 2, we investigated whether the pandemic subtype of influenza replaces or coexists with seasonal strains after the pandemic. The parameters appearing in the models in chapter 2 are the cross-immunity q between drifted strains of influenza and the basic

reproduction number $\mathcal{R}_0$ of seasonal influenza. We assumed the cross-immunity q at a reasonable level because there was no quantitative estimate of the cross-immunity so far. Since cross-immunity is a very important epidemiological parameter, a quantitative estimate of this parameter may be able to give more insight in the dynamics of influenza epidemics.

Kucharski et al. [56] developed a mechanistic model to measure cross-reactivity of antibodies to a challenging strain given a history of influenza A/H3N2 infection. They estimated that the exponential decay of cross-reactivity has the rate 0.29 per year. In the study by Kucharski et al. [56] there are two limitations. One is that they considered *in vitro* response (cross-reactivity), which does not always represent the *in vivo* response (cross-immunity), since the latter involves complex mechanisms in addition to antibody cross-reactivity. The second is that they assumed that cross-reactivity decays exponentially with time, implying that the strain in one season directly evolves from the strain of the previous season. The genetic evolution of these strains is commonly represented by a phylogenetic tree (see Viboud et al. [76], and section 1.3). Thus the antigenic change can be represented by a similar tree, called the evolutionary tree of antigens. The second assumption of Kucharski et al. [56] corresponds to a linear evolutionary tree of antigens.

We consider *in vivo* response with realistic evolutionary trees of antigens, and estimate the cross-immunity between strains of influenza A on the evolutionary tree. We develop a theoretical model that takes into account both the drift evolution (antigenic distance of influenza strains) and the cross-immunity gained from previous infections reducing the susceptibility to related strains of influenza. We fit our model to immune response data for influenza epidemics from the Seattle area for two seasons after the 1968 pandemic. We group influenza strains by their antigenic distance into a tree structure. Considering different evolutionary trees of antigens in our model, we determine the most likely structure during these seasons, which agrees with the observed tree structure found by Viboud et al. [76]. From our model, we also estimate the basic reproduction number of the pandemic influenza A/H3N2.

In section 3.2, we present the immune response data from the Seattle area after the 1968 pandemic. In section 3.3, we present an adapted theoretical model based on the seasonal model of section 2.2.3 to investigate the cross-immunity between influenza strains. Our statistical method for parameter estimation is presented in section 3.4; model validation and results are given in section 3.5. Discussion is given in section 3.6. Our main finding is that the cross-immunity between an influenza strain and its mutant is 88%. We also find the basic reproduction number of the 1968 pandemic influenza in line with previously

estimated values. This will appear as a paper: *S. M. Asaduzzman, Junling Ma, and P. van den Driessche. Estimation of cross-immunity between drifted strains of influenza A/H3N2. Bulletin of Mathematical Biology, accepted on November 01, 2017*

3.2 Sources of Data

The average cross-immunity in the population not only determines the attack rate of a seasonal epidemic [4, 7], but also depends on the attack rate of previous seasons. The attack rate in turn depends on the distribution of susceptibility in the population. It is difficult to estimate this distribution for seasonal epidemics, except for the seasons immediately following a pandemic. In the season following a pandemic, individuals are either completely susceptible to a challenging strain (those who escaped the pandemic) or have the same cross-immunity (those who were infected by the pandemic). This gives us the initial condition for our model of the evolution of the distribution of susceptibility. Thus we use the attack rates in the seasons immediately following the 1968 pandemic as given in Foy et al. [39, 40] for 1968–1971.

Foy et al. [39] conducted a field study among school children to evaluate the efficacy of a single dose of monovalent influenza vaccine. The study began in late November and early December of 1968 (Fig 3.1) by vaccinating junior high school children in the Seattle urban and suburban areas; a total of 4133 children were vaccinated with influenza A/Aichi/2/68(H3N2) or influenza B/Mass/66 strain on one occasion only. On a random basis, half of the children received influenza A vaccine (the study group) and half received influenza B vaccine. The children, who received influenza B vaccine, are taken as the control group, since influenza B vaccine is not effective against influenza A. At the time of vaccination, a random 20% of the children had blood samples collected, and vaccinated children were monitored for a period of three years. Following the pandemic that peaked in December 1968, blood samples were collected again in March 1969; see Fig 3.1 for the time line. An Influenza A/H3N2 strain caused a seasonal influenza epidemic during the influenza season of 1969–70. After this seasonal epidemic, blood samples were collected in March 1970 (Fig 3.1) for serological analyses and estimating infection rates among vaccinated children. A fourfold or greater titer rise in Complement Fixation or Hemagglutination Inhibition or both tests was taken as infection during the influenza season. A sample of 165 influenza A vaccine, and 152 influenza B vaccine recipients were tested for influenza infection in March 1970. There was no seasonal epidemic in the 1970–71 season in the Seattle urban and suburban areas [39]. Following the seasonal

A/H3N2 epidemic in the influenza season of 1971–72, blood samples were collected in March-April 1972; serological analyses of blood samples for influenza infection were based on 147 influenza A vaccine and 156 influenza B vaccine recipients. The results of serological analyses of blood samples are summarized in Table 3.1.

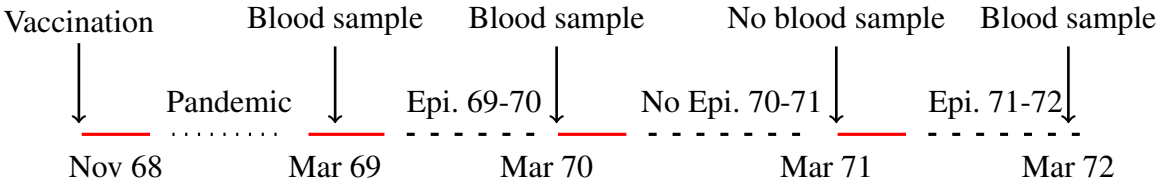

Figure 3.1: The time line of the A/H3N2 influenza study of Foy et al. [39, 40]. The dotted line indicates the duration of the pandemic influenza in 1968, the solid lines indicate the summer time between influenza epidemics, and the broken lines indicate the duration of typical seasonal influenza epidemics. Influenza vaccine was administered in November-December 1968; blood samples were collected in March 1969, March 1970 and March-April 1972.

Our method also depends on the pandemic attack rate in the general population, which is not available in Foy et al. [39, 40]. However, Davis et al. [28] provide this information in a similar high school population in another metropolitan area. Davis et al. [28] conducted a retrospective questionnaire survey among high school students and their families in the Kansas City area for histories of influenza like illness between November 1,1968 and January 17,1969 during the A/H3N2 influenza pandemic. On January 17, 1969 each student was requested to donate a blood sample for serologic studies of influenza infection. A total of 139 students out of 285 samples were found with antibody titers of at least $1:10$ of influenza A/H3N2, giving an estimate of 49% for the serologically confirmed attack rate of the pandemic.

Season	Influenza A vaccine (Study group)	Influenza B vaccine (Control group)
1969-70	10/165	33/152
1971-72	17/147	40/156

Table 3.1: The fraction of infected samples (number of infected children/number of total children in the group) from serological analyses after seasonal influenza A in the 1969–70 and 1971–72 influenza seasons (from Foy et al. [40], Table 4 and Foy et al. [39], Table 1).

3.3 Modeling the Dynamics of Seasonal Influenza

3.3.1 Population Model

We adapt a theoretical model from Andreasen's (2003) seasonal model presented in section 1.5.6 to investigate the cross-immunity between influenza strains depending on the evolutionary tree of antigens of influenza A/H3N2. We also adapt Andreasen's seasonal model in section 2.2.3, where we divided susceptible individuals into infinitely many classes according to their most recent infection year. Following the time line in Fig. 3.1, susceptible individuals are now divided into a few classes to fit the model to the influenza epidemic data in Table 3.1 for the 1969–70 and 1971–72 seasons in the Seattle area. We introduce the symbol S_ℓ^c as the fraction of susceptible individuals at the end of the current season c who had their last influenza in season ℓ, and S_0^c as the fraction of susceptible individuals at the end of the current season who have never been infected by the influenza A/H3N2 subtype.

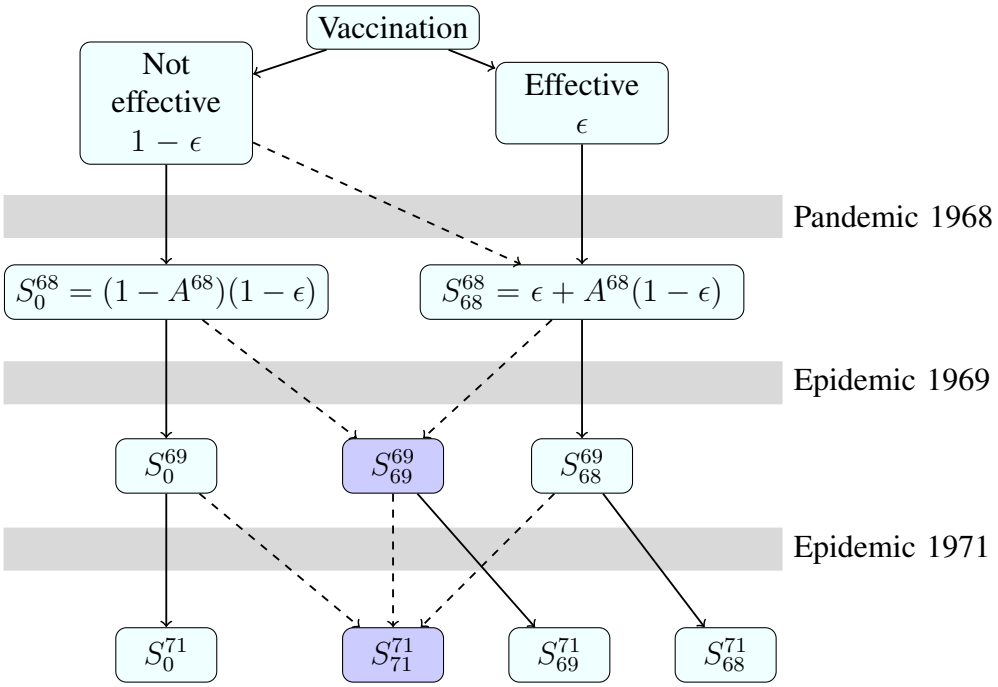

Figure 3.2: The progress of disease dynamics among the study group ($\epsilon > 0$), and the control group ($\epsilon = 0$). Here, A^{68} is the attack rate of the pandemic in 1968. The solid and dashed lines represent the flows of uninfected and infected individuals, respectively.

The flow of individuals among the S_ℓ^c classes is depicted in Fig. 3.2. Let ϵ be the proportion of individuals vaccinated who had an antibody response. For simplicity,

we assume that natural infection and effective vaccination have the same level of immunological response. Thus, after the pandemic in 1968, the S_{68}^{68} class contains individuals who were either effectively vaccinated or infected during the pandemic. That is

$$S_{68}^{68} = \epsilon + A^{68}(1-\epsilon)\,, \tag{3.1}$$

where A^{68} is the attack rate of the pandemic. In the vaccinated study group because everyone is vaccinated, ϵ is the fraction of vaccine recipients with an antibody response. For individuals who have no antibody response to the vaccine, a fraction $A^{68}(1-\epsilon)$ were infected by the pandemic, and a fraction

$$S_0^{68} = (1-A^{68})(1-\epsilon) \tag{3.2}$$

escaped the pandemic.

For $\ell \in \{0, 68\}$, the classes S_ℓ^{69} contain individuals in S_ℓ^{68} who escaped influenza in the 1969–70 season, and individuals who were infected during that season belong to S_{69}^{69}. We assume that a fraction of individuals ϕ_ℓ^{69} (with $0 < \phi_\ell^{69} < 1$) for $\ell \in \{0, 68\}$ in S_ℓ^{68} escaped influenza and a fraction $1-\phi_\ell^{69}$ were infected by influenza in the 1969–70 season. Thus,

$$\begin{aligned} S_\ell^{69} &= \phi_\ell^{69} S_\ell^{68}\,, \qquad \ell = 0, 68, & (3.3)\\ S_{69}^{69} &= 1 - \big(S_0^{69} + S_{68}^{69}\big). & (3.4) \end{aligned}$$

There was no observed influenza epidemic in the Seattle area in 1970–71 season [39], but an epidemic was observed in the 1971–72 season. Thus, similarly at the end of the 1971–72 epidemic season, individuals belonging to S_ℓ^{71} for $\ell \in \{0, 68, 69\}$ and S_{71}^{71} classes are found as follows

$$\begin{aligned} S_\ell^{71} &= \phi_\ell^{71} S_\ell^{69}\,, \qquad \ell = 0, 68, 69, & (3.5)\\ S_{71}^{71} &= 1 - \big(S_0^{71} + S_{68}^{71} + S_{69}^{71}\big), & (3.6) \end{aligned}$$

where ϕ_ℓ^{71} is the fraction of individuals in S_ℓ^{69} for $\ell \in \{0, 68, 69\}$ who escaped influenza infection during the 1971–72 season. Knowing the parameters ϵ, A^{68}, and ϕ_ℓ^{69} for $\ell \in \{0, 68\}$ and ϕ_ℓ^{71} for $\ell \in \{0, 68, 69\}$, the flow of individuals among S_ℓ^c classes are completely determined by (3.1)–(3.6). In Section 3.3.2, we model the transmission dynamics of seasonal influenza with an SIR-type model to determine the parameters ϕ_ℓ^{69} and ϕ_ℓ^{71}.

3.3.2 Seasonal Epidemic Model

We model the dynamics of seasonal influenza by taking into account an individual's infection history since this determines the cross-immunity of an individual to the challenging strain [4, 56]. Like Andreasen [4], we assume that the level of cross-immunity is determined by the most recent infection. We denote by $s_\ell^c(t)$ the fraction of susceptible individuals in season c at time t whose infection history belongs to ℓ, by $i(t)$ the fraction of infected and infectious individuals, and by $r(t)$ the fraction of recovered individuals. For $c = 69$, an individual's infection history ℓ belongs to $\{0, 68\}$, and $\ell \in \{0, 68, 69\}$ for $c = 71$. We ignore birth and death processes; thus $\sum_\ell s_\ell^c + i + r = 1$ is a constant. We assume that individuals in s_ℓ^c with $\ell \neq 0$ have susceptibility τ_ℓ^c. Individuals in s_0^c are assumed to have complete susceptibility, i.e., $\tau_0^c = 1$. We introduce non-dimensional time such that the infectious period is 1. The transmission dynamics of influenza for the season 1969–70 evolves according to the ordinary differential equations

$$\frac{ds_\ell^{69}}{dt} = -\mathcal{R}_0 \tau_\ell^{69} s_\ell^{69}\, i\,, \quad \ell = 0, 68, \tag{3.7a}$$

$$\frac{di}{dt} = \mathcal{R}_0\big(\tau_0^{69} s_0^{69} + \tau_{68}^{69} s_{68}^{69}\big) i - i\,, \tag{3.7b}$$

$$\frac{dr}{dt} = i\,. \tag{3.7c}$$

The initial conditions are $s_\ell^{69}(0) = S_\ell^{68}$ for $\ell \in \{0, 68\}$ (from Section 3.3.1), $i(0)$ is positive and small, and $r(0) = 0$. We assume that seasonal epidemics occur on a fast time scale, where the end of the epidemic is denoted by time ∞, thus $r(\infty) = S_{69}^{69}$ and $s_\ell^{69}(\infty) = S_\ell^{69}$. From (3.3), in this model $\phi_\ell^{69} = \frac{S_\ell^{69}}{S_\ell^{68}} = \frac{s_\ell^{69}(\infty)}{s_\ell^{69}(0)}$ for $\ell \in \{0, 68\}$. The final state of the seasonal epidemic can be calculated from (3.7a) by observing that

$$\frac{ds_{68}^{69}}{ds_0^{68}} = \tau_{68}^{69} \frac{s_{68}^{69}}{s_0^{69}}\,,$$

and integrating on the fast time scale from 0 to ∞ gives

$$\frac{s_{68}^{69}(\infty)}{s_{68}^{69}(0)} = \left(\frac{s_0^{69}(\infty)}{s_0^{69}(0)}\right)^{\tau_{68}^{69}}, \tag{3.8}$$

that is

$$\phi_{68}^{69} = \left(\phi_0^{69}\right)^{\tau_{68}^{69}}. \tag{3.9}$$

To determine ϕ_0^{69}, sum (3.7a)and (3.7b) and integrate from 0 to ∞

$$\begin{aligned} i(\infty) - i(0) + s_0^{69}(0)\big(\frac{s_0^{69}(\infty)}{s_0^{69}(0)} - 1\big) \quad + \\ s_{68}^{69}(0)\big(\frac{s_{68}^{69}(\infty)}{s_{68}^{69}(0)} - 1\big) \quad = \quad \frac{1}{\mathcal{R}_0}\int_0^\infty \frac{1}{s_0^{69}(t)}\frac{ds_0^{69}}{dt}dt\,. \end{aligned} \tag{3.10}$$

At the beginning of the epidemic, $i(0)$ is very small, so it can be taken as zero, and at the end of the epidemic $i(\infty)$ is zero because no one is infectious anymore. Thus using (3.9), the final size equation from (3.10) can be written as

$$\begin{aligned} \log(\phi_0^{69}) &= \mathcal{R}_0\big(s_0^{69}(0)\big[\phi_0^{69} - 1\big] + s_{68}^{69}(0)\big[(\phi_0^{69})^{\tau_{68}^{69}} - 1\big]\big) \\ &= \mathcal{R}_0\big(S_0^{68}\phi_0^{69} + S_{68}^{68}(\phi_0^{69})^{\tau_{68}^{69}} - 1\big). \end{aligned} \tag{3.11}$$

Similarly, using $s_\ell^{71}(0) = S_\ell^{69}$ for $\ell \in \{0, 68, 69\}$, it follows that

$$\phi_\ell^{71} = \left(\phi_0^{71}\right)^{\tau_\ell^{71}}, \quad \ell = 68, 69, \tag{3.12}$$

and

$$\log(\phi_0^{71}) = \mathcal{R}_0\big(S_0^{69}\phi_0^{71} + S_{68}^{69}(\phi_0^{71})^{\tau_{68}^{71}} + S_{69}^{69}(\phi_0^{71})^{\tau_{69}^{71}} - 1\big). \tag{3.13}$$

With (3.9), (3.11)–(3.13), equations (3.3)–(3.6) determine S_ℓ^{69} and S_ℓ^{71} once τ_ℓ^{69} and τ_ℓ^{71} are modeled; see Section 3.3.3.

3.3.3 Evolutionary Trees of Antigens

Fig. 3.3 lists all possible canonical evolutionary trees of antigens of influenza A/H3N2 for the strains appearing in the 1969–70 and 1971–72 seasons, rooted at the 1968 pandemic strain. A node a represents the influenza strain in year a that caused an epidemic, and an arc connects from node a to node b if strain b evolves from strain a and causes an epidemic in year b. We define the unit antigenic distance as the average number of epitopes between two strains connected by an arc. Thus, the antigenic distance $d(c, \ell)$ is the number of arcs between the nodes c and ℓ on the evolutionary tree of antigens. For example in Fig. 3.3, Model 1 assumes that the 69 strain is a mutant of (i.e., evolves from) the 68 strain, and the 71 strain is a mutant of the 68 strain, with $d(68, 69) = 1$ and $d(68, 71) = 2$. Model 2 assumes that the 71 strain is a mutant of some $70'$ strain that did not appear in the Seattle

area, which is a mutant of the 69 strain. Model 3 assumes that the 69 and 71 strains are independent mutants of the 68 strain, and in Models $4-5$ the 71 strain is a descendant of some $70'$ strain that did not appear in the Seattle area; thus for instance in Model 5, $d(68,71)=3$ and $d(69,71)=4$.

We assume, as Boni et al. [13] and Kucharski et al. [56], that the cross-immunity decays exponentially with antigenic distance. This gives $\tau_\ell^c = 1-q^{d(c,\ell)}$ as the susceptibility in the current season c, where q is the cross-immunity between strains connected by an arc. With parameters ϵ, q, $\mathcal{R}_0$ and A^{68} and the evolutionary tree, the flow in Fig. 3.2 is uniquely determined.

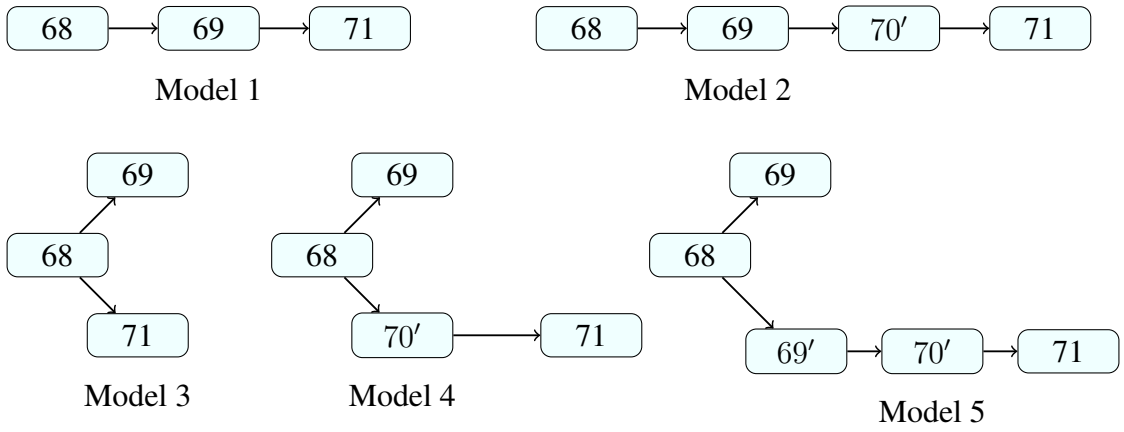

Figure 3.3: Possible evolutionary tree of antigens of influenza A/H3N2 after the 1968 pandemic. The prime $'$ indicates a strain that did not appear in the Seattle area.

3.4 Statistical Method for Parameter Estimation

We use the maximum likelihood method to estimate the cross-immunity q between influenza strains depending on the tree of A/H3N2 with unit antigenic distance, the vaccine protection ϵ against the vaccinating strain, the basic reproduction number $\mathcal{R}_0$, and the attack rate of the 1968 pandemic A^{68} by fitting the model of Section 3.3 to the four data points in Table 3.1. We assume that each individual has the same probability of being infected during the pandemic influenza or seasonal influenza after the pandemic. Denote by X^{68} the number of infected individuals in a sample of size N during the pandemic. Thus X^{68} follows a Binomial distribution with parameter A^{68} and sample size N, i.e., $X^{68} \sim \text{BIN}(N, A^{68})$, where X^{68} and N are respectively 139 and 285 from Davis et al. [28]; see Section 3.2.

Let X^c and $\tilde{X}^c$ be the number of infected individuals among influenza A and influenza B vaccinated individuals (control group) in a sample of size N^c and $\tilde{N}^c$ in a season c, where $c = 69$ for the 1969-70 season and $c = 71$ for the 1971-72 season. The numerator and denominator of the first column of Table 3.1 correspond to X^c and N^c, and the numerator and denominator of the second column of Table 3.1 correspond to $\tilde{X}^c$ and $\tilde{N}^c$ for a season c. We determine the attack rate of seasonal influenza in the 1969–70 and 1971–72 seasons in the influenza A vaccine recipient ($\epsilon > 0$) and influenza B vaccine recipient ($\epsilon = 0$) populations and taking these attack rates as a probability of infection during the seasonal influenza, $X^{69} \sim \text{BIN}(N^{69}, S_{69}^{69})$, $X^{71} \sim \text{BIN}(N^{71}, S_{71}^{71})$ and $\tilde{X}^{69} \sim \text{BIN}(\tilde{N}^{69}, \tilde{S}_{69}^{69})$, $\tilde{X}^{71} \sim \text{BIN}(\tilde{N}^{71}, \tilde{S}_{71}^{71})$, where $\tilde{S}_{69}^{69}$ and $\tilde{S}_{71}^{71}$ denote the attack rates of seasonal influenza among influenza B vaccinated individuals in the 1969–70 and 1971–72 season. The log likelihood function of the parameters q, ϵ,$\mathcal{R}_0$ and A^{68} is

$$\begin{aligned}\mathcal{L}(q, \epsilon, \mathcal{R}_0, A^{68}) &= \log\big(F(X^{69}; N^{69}, S_{69}^{69})\big) + \log\big(F(X^{71}; N^{71}, S_{71}^{71})\big) \\ &+ \log\big(F(\tilde{X}^{69}; \tilde{N}^{69}, \tilde{S}_{69}^{69})\big) + \log\big(F(\tilde{X}^{71}; \tilde{N}^{71}, \tilde{S}_{71}^{71})\big) \\ &+ \log\big(F(X^{68}, N, A^{68})\big)\,, \end{aligned} \tag{3.14}$$

where $F(X; N, p)$ is the probability mass function of a Binomial random variable. We find the set of parameters for influenza A/H3N2 that maximizes the log likelihood function $\mathcal{L}$ in (3.14) by using Matlab fmincon function. The Akaike information criterion

$$\text{AIC} = 2(k - \mathcal{L})\,,$$

where k is the number of parameters ($k = 4$), is computed for the relative quality of the models for the data in Table 3.1. The 95% confidence interval for the parameters is found from the likelihood ratio test; see, for example, [8, pp. 417-422].

3.5 Model Validation and Results

The point estimates of the parameters of the models in Fig. 3.3 (with their corresponding τ_ℓ^c) and their AIC are summarized in Table 3.2. Among the candidate models in Fig. 3.3, the preferred model (minimum AIC) is Model 5. These five models have the same number of parameters, so the order of Bayesian information criterion (BIC) is the same as that for AIC. Viboud et al. [76] presented an evolutionary tree for the influenza H3 gene during the period including 1968–1972. This suggests that the 69 and 71 strains are two different

branches of the 68 strain. Our best fit evolutionary tree of antigens agrees with that of the evolutionary tree of the H3 gene but differs from that of the N2 gene, given by Viboud et al. [76, Fig. 4].

	Point estimate				
Model	ϵ	q	$\mathcal{R}_0$	A^{68}	AIC
1	1.00	0.70	1.74	0.49	41.55
2	1.00	0.85	2.05	0.49	36.51
3	1.00	0.47	1.46	0.49	51.00
4	1.00	0.81	1.95	0.49	35.70
5	0.99	0.88	2.15	0.49	34.93

Table 3.2: Point estimates of the parameters of the Models in Fig. 3.3 and their AIC.

From the data in Table 3.1 and the susceptibility structure of the best fit evolutionary tree of antigens (Model 5, Fig. 3.3), we estimate that the cross-immunity between influenza strains with unit antigenic distance q is 88% (85–91%), the vaccine protection against the vaccinating strain ϵ is 99% (65–100%), the basic reproduction number $\mathcal{R}_0$ is 2.15 (1.84–2.59), and the attack rate of the pandemic A^{68} is 49% (42–56%). The likelihood profile of the parameters is shown in Fig. 3.4. The point and interval estimates of the parameters are summarized in Table 3.3, with the distribution of the attack rate for each season given in Fig. 3.5.

Parameter	Point estimate	95% Confidence Interval
ϵ	0.99	0.65–1.00
q	0.88	0.85–0.91
$\mathcal{R}_0$	2.15	1.84–2.59
A^{68}	0.49	0.42–0.56

Table 3.3: Point and interval estimates of the parameters for A/H3N2.

Since there was no observable epidemic in the Seattle area in the 1970–71 season, the strain $70'$ may be a descendent of strain 69, 68 or $69'$ (the latter is depicted in Model 5). Our estimated parameters yield a very small attack rate in the 1970–71 influenza season (Fig. 3.5 (a), (b), (c)); agreeing with the observation of Foy et al. [39] that there was no observable epidemic in the 1970–71 season.

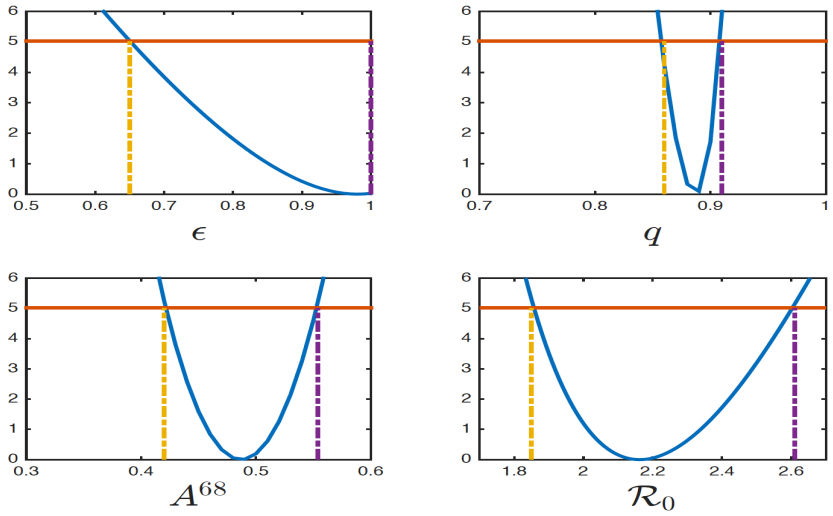

Figure 3.4: The plots give the likelihood ratio when varying the single parameter on the horizontal axis. The dashed vertical lines mark the 95% confidence limits.

3.6 Discussion

We used a novel statistical model to investigate the cross-immunity between strains of influenza A/H3N2. Our model incorporated the knowledge of the immune status of susceptible individuals depending on the evolutionary tree of antigens of influenza A/H3N2. The value of the cross-immunity between an influenza strain and its mutant strains implies that an individual infected by a strain has 12% probability of infection by a mutant strain in the next seasonal epidemic. We also determined that the vaccine is highly effective in inducing an immune response. Thus, a vaccinated individual can expect an infection with probability ≤ 0.01 if the season's influenza outbreak is caused by the vaccinating strain. Cross-immunity is a better measure of vaccine protection than vaccine efficacy because the latter depends on factors that are not related to the vaccine, for example, the probability of individuals in an unvaccinated population being challenged by the circulating strain.

In a study of individuals tested against nine different influenza A/H3N2 strains isolated between 1968 and 2008, Kucharski et al.[56] found a value $e^{-0.29} \approx 0.75$ corresponding to our q, which is lower than the range in Table 3.3. This may be because we focused only on years following the 1968 pandemic, and strains from consecutive seasons may be on different branches of the evolutionary tree (Model 5) resulting in a smaller cross-immunity between seasons. In addition, *in vivo* cross-immunity is expected to be larger than *in vitro* cross-immunity because of more types of immune response.

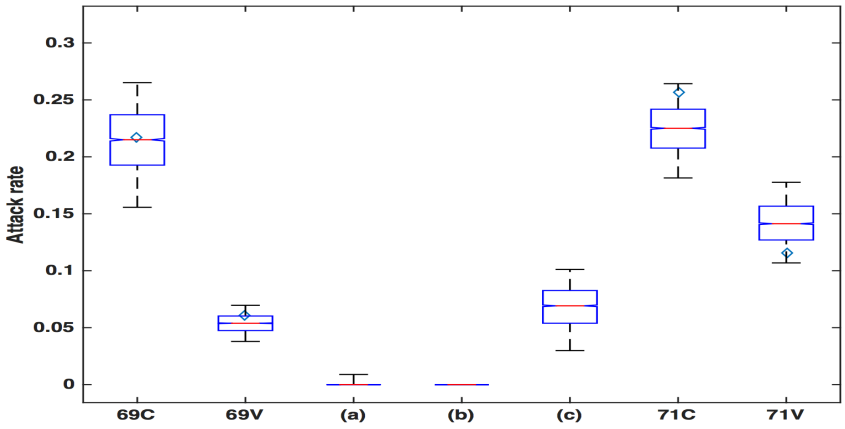

Figure 3.5: The distribution of the influenza A/H3N2 attack rates are given by boxplots, where the whiskers represent the 95% confidence intervals. The observed attack rates in the seasons 1969–70 and 1971–72 are depicted with a diamond $\diamond$ symbol (given in Table 3.1). The labels 69C, 71C and 69V, 71V represent control and vaccinated groups of individuals in these years. For the 1970–71 season, the strain that may have challenged in the Seattle area could be (a) a descendant of the 69 strain as in Model 2, (b) a descendant of the 68 strain as in Model 4 or (c) a descendant of some $69'$ strain and the parent of the 71 strain as in Model 5.

The basic reproduction number $\mathcal{R}_0$ of the 1968 pandemic influenza that we estimated agrees with previously estimated values of $1.5-2.2$ in [21] and $1.60-2.12$ in [52]. The data that we used are for school children, who have higher contact rates than other age groups. So we expect that the attack rate and the basic reproduction number would be lower in a general population.

Our model assumes that the antigenic drift in each season is the same. However, some theoretical studies (e.g., Boni et al. [13]) suggest that the antigenic drift of the pandemic strain is larger than that of the seasonal strain of influenza because the pandemic has a much greater attack rate. Our model also assumes that the effectiveness of the vaccine is all-or-nothing. However, the vaccine could be leaky [46], i.e, every vaccinated individual is protected to some extent, but has a probability of infection. Note that both these alternative hypotheses reduce the cross-immunity between the pandemic strain and a 69 strain. We model these by assuming the cross-immunity between the 68 and 69 $(69')$ strain is equal to γq, where $\gamma \in [0,1]$. If the antigenic drift in the 1968 pandemic is larger, then the cross-immunity between the 69 and 71 strains becomes $\gamma^2 q^4$ in Model 5. On the other hand, if the vaccine is leaky the cross-immunity of the individuals infected in the 1969 season remains q^4 for Model 5. For simplicity, we assume that the vaccine is effective for all individuals, i.e., $\epsilon = 1$ for Model 5 with either hypothesis. Running Model 5 with either

hypothesis, the point estimates of the parameters remain identical with the values given in Table 3.3, and $\gamma = 1$. Thus, our model cannot distinguish these hypotheses, but they do not affect our estimates of cross-immunity q, and the basic reproduction number $\mathcal{R}_0$.

Our theoretical model connects the susceptibility distribution with the influenza evolutionary tree of antigens. Thus a variant of our model in Section 3.3 can be used to study the evolution of influenza after any pandemic. Our findings of cross-immunity between influenza strains can be used to compute the basic reproduction number (fitness) of the challenging strain. This information may be helpful for predicting which strain of influenza may cause the next season's epidemic, and give better suggestions for the composition of a seasonal influenza vaccine.

Chapter 4

Modeling the Dynamics of Pandemic Influenza with Contact Heterogeneity

4.1 Introduction

We modeled the dynamics of pandemic influenza in section 2.2.2 by assuming a homogeneous mixing of individuals to study the replacement or coexistence of seasonal subtype by the pandemic subtype. Qualitatively our model may be able to explain the replacement of the seasonal subtype H1N1 by the pandemic subtype H2N2 in 1957. The pandemic subtype H2N2 was a reassortment from H1N1 [34, 78]. Thus it is reasonable to assume that the cross-immunity between this pandemic subtype and the seasonal subtype H1N1 was at an intermediate level. The pandemic subtype H3N2 in 1968, also a reassortment from the previous subtype H2N2 [34, 78], similarly replaced the seasonal subtype H2N2. The subtype H1N1 was not directly descended from H3N2, thus in 1977 the cross-immunity between the pandemic subtype H1N1 and the prevailing seasonal subtype H3N2 could be weak, leading to their coexistence. Qualitatively the hybrid model, formulated in chapter 2, for the dynamics of influenza A epidemics agrees with the above observations.

We now investigate whether the pandemic influenza model in section 2.2.2 quantitatively agrees with the pandemic outcomes such as the attack rate. In section 2.2.1, we assumed that individuals who recovered from the pandemic influenza gain stronger cross-immunity and become less susceptible to the seasonal influenza. Thus, the model for the dynamics of pandemic influenza needs to estimate the observed pandemic attack rate correctly. Without this, the condition under which the pandemic subtype replaces or coexists with the seasonal

subtype does not reflect the true condition.

Numerical simulation in section 2.3.2 shows that approximately 5–6$\%$ individuals (individuals in S_0^*) have never been infected by the seasonal influenza. Thus neglecting S_0^*, the reproduction number of the pandemic influenza in (2.4) and its attack rate in (2.8) become $\mathcal{R}_p = p\mathcal{R}_{0_p}$ and $Z = 1 - \psi^p$ respectively, where ψ^p satisfies

$$\log(\psi^p) = \mathcal{R}_p(\psi^p - 1). \tag{4.1}$$

In chapter 3, the basic reproduction number $\mathcal{R}_p$ of the 1968 pandemic influenza is found to be 2.15 (1.84–2.59), and serologically confirmed attack rate to be in the range 42–56$\%$ by taking the value 49$\%$ from Davis et al. [28]. Matching $\mathcal{R}_p$ with the basic reproduction number of the 1968 pandemic influenza, the attack rate Z from (4.1) is found to be 75-90$\%$. For the pandemics in the last century, a symptomatic attack rate 24–35$\%$ has been reported by many authors (e.g., Biggerstaff et al. [11], Gani et al. [41]). Thus, the attack rate found from (4.1) is much higher than the symptomatic attack rate published in the literature [11, 41]; it is also higher than the serologically confirmed attack rate 42–56$\%$ that we found in chapter 3. Conversely, if the attack rate from the model falls between the range 42–56$\%$, the basic reproduction number falls in the range 1.32–1.50, which is much lower than the range we found in chapter 3. Thus, the attack rate from the model in section 2.2.2 is an overestimation.

Contact rates are age specific; some individuals of the population make more contacts than others. Meyers et al. [60] confirmed that school aged children have the maximum number of average contacts, followed by working adults; contact rates of non-working adults are the minimum. Thus, individuals of different age have different susceptibility. These age-related distinctions are necessary to assess vaccination strategies. For example, vaccinating school aged children could lower the overall attack rate [20]. Brauer [14] showed that the attack rate of influenza from a one group model with homogeneous mixing is higher than the attack rate from a two group model with heterogeneous mixing. Also, Ball [9] showed that the final size decreases in the transmission dynamics of epidemics for individuals with heterogeneous susceptibilities.

Following these, we modify the pandemic model in section 2.2.2 by incorporating contact rate heterogeneity of individuals with the possibility of lowering the attack rate of the pandemic influenza. In section 4.3.1, we model the dynamics of pandemic influenza with constant susceptibility to the pandemic, and in section 4.4, the model is extended to incorporate infection history dependent susceptibility to the pandemic. We explore

whether the contact rate heterogeneity in the dynamics of the pandemic influenza gives the attack rate in the observed range. Since no quantitative match is found, our finding suggests that the attack rate of a future 1968-like pandemic influenza might have resulted from a combination of other mechanisms, such as seasonal change in transmission rate or behavioral change of individuals during the pandemic.

4.2 Source of Data

We obtained contact network data for the Greater Vancouver Metropolitan area from Conway et al. [20], who used the same data as Meyers et al. [60]. Conway et al. [20] used an extended SIR-type model including heterogeneity in age and contact rates to assess the impact of vaccination and the timing of the vaccination campaign in limiting influenza incidence against the 2009 pandemic influenza. Individuals in the Greater Vancouver Metropolitan area were segregated according to age and degree (number of weekly contacts) groups to capture realistic demographic effects. Eight different age groups: 0–2, 3–4, 5–18, 19–24, 25–54, 55–64, 65+ and 65+ in long-term care, and five degree groups: 0–5, 6–15, 16–30, 31–100 and 100+ contacts per week were considered. The degree group with 100+ contacts per week was taken to represent health care workers, who are more likely to receive and transmit infection. For each age group k and degree group ℓ, Conway et al. [20] found the fraction of individuals belonging to that age and degree group, and also the average number of contacts per week. The fractions of contacts for age group k and degree group ℓ were arranged in a 8×5 matrix, whose (u, v) entry represents the fraction of contacts of an individual in age group k and degree group ℓ with individuals in age group u and degree group v. There are 40 such matrices, each has the sum of entries equal to 1. Denote by $M(k, \ell)$ the matrix of the fraction of contacts of an individual in age group k and degree group ℓ with all other age and degree groups. The average contacts of an individual in age group k and degree group ℓ is denoted by $K_{k\ell}$, and the population weight in that age and degree group is denoted by $P_{k\ell}$, giving matrices K and P used in section 4.3.3.

4.3 Dynamics of Pandemic Influenza

4.3.1 Heterogeneous Mixing of Individuals with Constant Susceptibility to the Pandemic

In an attempt to understand the mechanism that lowers the attack rate of the pandemic influenza, we adapt the SIR-type model in section 2.2.2 to incorporate contact rate heterogeneity of individuals in the dynamics of pandemic influenza. To use the data described in section 4.2, we divide the total population N into n contact groups. Denote by N_k the number of individuals in contact group k for $k = 1, 2, \ldots, n$ with $\sum_{k=1}^{n} N_k = N$. Thus, if the contact group k represents an age group or an age and degree group as in Conway et al. [20], the value of n is either 8 or 40. We assume that individuals in contact group k belong to one of the three classes: susceptible (S_k), infected and infectious (I_k) and recovered (R_k). Susceptible individuals in S_k are divided into sub-classes according to their most recent infection year. Denote by S_{k0} the number of S_k individuals who have never been infected by seasonal influenza, and S_{ki} for $i \geq 1$ the number of S_k individuals who were infected by seasonal influenza i years ago. Thus, the individuals in contact group k is $N_k = \sum_i S_{ki} + I_k + R_k$.

As assumed in section 2.2.1, individuals recovering from an influenza infection gain partial cross-immunity to the related strains of influenza [30, 42]. A pandemic subtype usually results from the recombination of gene segments of avian viruses with human influenza virus [10]. Thus, we assume that individuals who were infected by seasonal influenza have some cross-immunity to the pandemic subtype. Assuming that cross-immunity reduces susceptibility, we assume that all the individuals (except those in S_{k0}) have the same level of susceptibility p to the pandemic influenza. As in section 2.2.2, the cross-immunity between the pandemic subtype and any seasonal strain of influenza is $(1 - p)$. We ignore birth and death processes in the dynamics of the pandemic influenza, thus N_k is a constant for contact group k. We denote by β_{kj} the transmission rate between an individual in contact group j to an individual in contact group k, and by α the recovery rate from the pandemic influenza. For $k = 1, 2, \ldots, n$, the transmission dynamics of the

pandemic influenza evolves according to the following ODEs

$$\frac{dS_{k0}}{dt} = -S_{k0}\sum_{j=1}^{n}\beta_{kj}I_j\,, \tag{4.2a}$$

$$\frac{dS_{ki}}{dt} = -pS_{ki}\sum_{j=1}^{n}\beta_{kj}I_j\,, \qquad i=1,2,\ldots, \tag{4.2b}$$

$$\frac{dI_k}{dt} = \big(\sum_{j=1}^{n}\beta_{kj}I_j\big)\big(\sum_{i=1}^{\infty}pS_{ki}+S_{k0}\big)-\alpha I_k\,, \tag{4.2c}$$

$$\frac{dR_k}{dt} = \alpha I_k\,. \tag{4.2d}$$

The initial conditions are $S_{ki}(0)=S^*_{ki}$ with $\sum_{k=1}^{n}\sum_{i=0}^{\infty}S^*_{ki}\approx N$, and $I_k(0)$ is small and positive and $R_k(0)=0$. Here, S^*_{ki} is the number of susceptible individuals before the pandemic subtype causes an outbreak.

Basic Reproduction Number

Using the next generation matrix [75], the basic reproduction number is $\mathcal{R}_{0_p}=\rho\big(FV^{-1}\big)$, where $\rho(.)$ is the spectral radius of a square matrix. We skip the details of the matrices F and V (see van den Driessche et al. [75]). For the model (4.2), the matrix F can be written as the product of two matrices T and B, where

$$T=\begin{bmatrix}\sum_{i=1}^{\infty}pS_{1i}(0)+S_{10}(0) & 0 & \ldots & 0\\ 0 & \sum_{i=1}^{\infty}pS_{2i}(0)+S_{20}(0) & \ldots & 0\\ \vdots & \vdots & \ddots & \vdots\\ 0 & 0 & \ldots & \sum_{i=1}^{\infty}pS_{ni}(0)+S_{n0}(0)\end{bmatrix} \tag{4.3}$$

and

$$B=\begin{bmatrix}\beta_{11} & \beta_{12} & \ldots & \beta_{1n}\\ \beta_{21} & \beta_{22} & \ldots & \beta_{2n}\\ \vdots & \vdots & \ddots & \vdots\\ \beta_{n1} & \beta_{n2} & \ldots & \beta_{nn}\end{bmatrix}. \tag{4.4}$$

Also, the matrix V is given by

$$V = \begin{bmatrix} \alpha & 0 & \dots & 0 \\ 0 & \alpha & \dots & 0 \\ \vdots & \vdots & \ddots & \vdots \\ 0 & 0 & \dots & \alpha \end{bmatrix}.$$

We assume that the distribution of susceptible individuals in each contact group is the same. Define $s_i^* = \frac{S_{ki}^*}{N_k}$ for $k = 1, 2, \dots, n$, and assume that the distribution of susceptible individuals s_i^* has reached an equilibrium with $\sum_{i=0}^{\infty} s_i^* = 1$ before the outbreak of the pandemic. Using the initial conditions $S_{ki}(0) = S_{ki}^* = N_k s_i^*$ for $k = 1, 2, \dots, n$, the matrix T in (4.3) can be written as

$$\begin{aligned} T &= \begin{bmatrix} N_1\big(\sum_{i=1}^{\infty} p s_i^* + s_0^*\big) & 0 & \dots & 0 \\ 0 & N_2\big(\sum_{i=1}^{\infty} p s_i^* + s_0^*\big) & \dots & 0 \\ \vdots & \vdots & \ddots & \vdots \\ 0 & 0 & \dots & N_n\big(\sum_{i=1}^{\infty} p s_i^* + s_0^*\big) \end{bmatrix} \\ &= \begin{bmatrix} N_1\big(p(1-s_0^*) + s_0^*\big) & 0 & \dots & 0 \\ 0 & N_2\big(p(1-s_0^*) + s_0^*\big) & \dots & 0 \\ \vdots & \vdots & \ddots & \vdots \\ 0 & 0 & \dots & N_n\big(p(1-s_0^*) + s_0^*\big) \end{bmatrix} \\ &= N\big(p(1-s_0^*) + s_0^*\big) \begin{bmatrix} a_1 & 0 & \dots & 0 \\ 0 & a_2 & \dots & 0 \\ \vdots & \vdots & \ddots & \vdots \\ 0 & 0 & \dots & a_n \end{bmatrix}, \end{aligned} \tag{4.5}$$

where $a_k = \frac{N_k}{N}$ is the fraction of individuals in contact group k. Denote by D the diagonal matrix whose kth diagonal entry is the population weight of contact group k, i.e., $D = \text{diag}(a_1, \dots, a_n)$. Using D in (4.5), the matrix T can be written as $T = N\big(p(1-s_0^*)+s_0^*\big)D$. Thus, the basic reproduction number $\mathcal{R}_{0_p}$ is given by

$$\mathcal{R}_{0_p} = \frac{N\big(p(1-s_0^*) + s_0^*\big)}{\alpha} \rho(DB). \tag{4.6}$$

Final Size Relation

We divide (4.2b) by (4.2a), and (4.2a) by S_{k0}; then integrate from the beginning of the pandemic at $t = 0$ to the end of the pandemic at $t = \infty$ to obtain

$$\log\left(\frac{S_{ki}(\infty)}{S_{ki}(0)}\right) = p\log\left(\frac{S_{k0}(\infty)}{S_{k0}(0)}\right), \tag{4.7}$$

and

$$\log\left(\frac{S_{k0}(\infty)}{S_{k0}(0)}\right) = -\sum_{j=1}^{n}\beta_{kj}\int_0^\infty I_j(t)dt. \tag{4.8}$$

Denote by $\psi_k = \frac{S_{k0}(\infty)}{S_{k0}(0)}$ the fraction of individuals in contact group k who have never been infected by seasonal influenza and escaped the pandemic infection. Using ψ_k in (4.7), the fraction of individuals in contact group k who had seasonal influenza i seasons before and escaped the pandemic is given by $\frac{S_{ki}(\infty)}{S_{ki}(0)} = \psi_k^p$. The integral $\int_0^\infty I_j(t)dt$ in (4.8) is the total number of individuals infected during the pandemic in contact group j; to find the integral $\int_0^\infty I_j(t)dt$, add (4.2a)–(4.2c) and integrate from 0 to ∞ giving

$$\begin{aligned}
\frac{dS_{k0}}{dt} + \sum_{i=1}^{\infty}\frac{dS_{ki}}{dt} + \frac{dI_k}{dt} &= -\alpha I_k\,, \\
S_{k0}(\infty) - S_{k0}(0) + \sum_{i=1}^{\infty}\big(S_{ki}(\infty) - S_{ki}(0)\big) + I_k(\infty) - I_k(0) &= -\alpha\int_0^\infty I_k(t)dt. \qquad (4.9)
\end{aligned}$$

The dynamics of the pandemic influenza in each contact group k evolves according to the model (4.2a)–(4.2d), and at the end of the pandemic $I_k(\infty)$ is approximately close to zero since no one is infected anymore. Thus, using the initial conditions with $I_k(0) \approx 0$, equation (4.9) for contact group j becomes

$$\begin{aligned}
S_{j0}(0)\big(1 - \frac{S_{j0}(\infty)}{S_{j0}(0)}\big) + \sum_{i=1}^{\infty} S_{ji}(0)\big(1 - \frac{S_{ji}(\infty)}{S_{ji}(0)}\big) &= \alpha\int_0^\infty I_j(t)dt \\
\frac{1}{\alpha}\big[N_j s_0^*(1-\psi_j) + \sum_{i=1}^{\infty} N_j s_i^*(1-\psi_j^p)\big] &= \int_0^\infty I_j(t)dt. \qquad (4.10)
\end{aligned}$$

Substituting $\int_0^\infty I_j(t)dt$ in (4.8), the final size relation becomes

$$\begin{aligned}\log(\psi_k) &= -\sum_{j=1}^{n} \frac{N_j\beta_{kj}}{\alpha}\big(s_0^*(1-\psi_j)+(1-s_0^*)(1-\psi_j^p)\big) \\ &= -\frac{N}{\alpha}\sum_{j=1}^{n} a_j\beta_{kj}\big(s_0^*(1-\psi_j)+(1-s_0^*)(1-\psi_j^p)\big), \end{aligned} \tag{4.11}$$

for $k = 1, 2, \ldots, n$, where $a_j\beta_{kj}$ is the total infection from all individuals in contact group j to an individual in contact group k.

Attack Rate of the Pandemic

The attack rate (see section 1.5.1) of the pandemic influenza is the overall fraction of individuals infected during the pandemic influenza, which is defined as

$$\begin{aligned} Z &= 1 - \frac{\sum_{k=1}^{n}\big[S_{k0}(\infty)+\sum_{i=1}^{\infty}S_{ki}(\infty)\big]}{N} \\ &= 1 - \frac{\sum_{k=1}^{n}\big[S_{k0}(0)\psi_k+\sum_{i=1}^{\infty}S_{ki}(0)\psi_k^p\big]}{N} \\ &= 1 - \sum_{k=1}^{n}\frac{N_k}{N}\big[s_0^*\psi_k+\sum_{i=1}^{\infty}s_i^*\psi_k^p\big] \\ &= 1 - \sum_{k=1}^{n} a_k\big[s_0^*\psi_k+(1-s_0^*)\psi_k^p\big]. \end{aligned} \tag{4.12}$$

4.3.2 Reduction of the Model in Section 4.3.1

Since we assume that all the individuals (except individuals in S_{k0}) have the same susceptibility p to the pandemic influenza, we can reduce the model (4.2) to four differential equations for each $k = 1, 2, \ldots, n$. Define $V_k = \sum_{i=1}^{\infty} S_{ki}$; then the transmission dynamics of

the pandemic influenza for the model (4.2) can be written as following

$$\frac{dS_{k0}}{dt} = -S_{k0}\sum_{j=1}^{n}\beta_{kj}I_j\,, \tag{4.13a}$$

$$\frac{dV_k}{dt} = -pV_k\sum_{j=1}^{n}\beta_{kj}I_j\,, \tag{4.13b}$$

$$\frac{dI_k}{dt} = (pV_k + S_{k0})\sum_{j=1}^{n}\beta_{kj}I_j - \alpha I_k\,, \tag{4.13c}$$

$$\frac{dR_k}{dt} = \alpha I_k\,. \tag{4.13d}$$

The initial conditions are $S_{k0}(0) = N_k s_0^*$, $V_k(0) = N_k(1 - s_0^*)$, and $I_k(0)$ is small and positive and $R_k(0) = 0$. The basic reproduction number is the same as in (4.6). With this notation, equation (4.7) and (4.9) takes the form

$$\log\left(\frac{V_k(\infty)}{V_k(0)}\right) = p\log\left(\frac{S_{k0}(\infty)}{S_{k0}(0)}\right),$$

and

$$S_{k0}(\infty) - S_{k0}(0) + V_k(\infty) - V_k(0) + I_k(\infty) - I_k(0) = -\alpha\int_0^\infty I_k(t)dt.$$

Using initial conditions of the model (4.13), the final size relation is the same as in (4.11).

4.3.3 Numerical Simulation

We numerically simulate the model (4.2) to determine the pandemic influenza attack rate Z in (4.12), which is a functions of ψ_k for $k = 1, 2, \ldots, n$. To find ψ_k, we need to solve the system of non-linear equations in (4.11), which involve the fraction of susceptible individuals s_i^* who had seasonal influenza i years before. Following the numerical procedure in section 2.3.2, and using the determined values of cross-immunity q and basic reproduction number $\mathcal{R}_0$ of the 1968 pandemic influenza from chapter 3, we find s_i^* values by solving the season-to-season mapping equations (2.13)–(2.15); uniqueness of s_i^* is established in section 2.3.2.

The final size equations in (4.11), and the basic reproduction number in (4.6) are functions of transmission rates β_{kj}, for $k = 1, 2, \ldots, n$ and $j = 1, 2, \ldots, n$. The transmission rates β_{kj} are very difficult to determine; however β_{kj} is the product of the

contact rate between an individual in contact group j and an individual in contact group k, and the probability of disease transmission $\eta \in [0,1]$ from the contact. The value $\eta = 0$ indicates that the disease is never transmitted, and $\eta = 1$ implies that each contact transmits disease from an infectious individual to a susceptible individual.

Denote by c_{kj} the contact rate between an individual in contact group k to all individuals in contact group j. With this notation, the contact rate c_{kj} and transmission rate β_{kj} are related by the equation

$$a_j \beta_{kj} = \eta c_{kj} \,, \tag{4.14}$$

where a_j is the fraction of individuals in contact group j, determined from population census data. Using the contact rate relation in (4.14), the transmission rate matrix B in (4.4) can be written as follows

$$\begin{aligned} B &= \eta \begin{bmatrix} c_{11} & c_{12} & \dots & c_{1n} \\ c_{21} & c_{22} & \dots & c_{2n} \\ \dots & \dots & \dots & \dots \\ c_{n1} & c_{n2} & \dots & c_{nn} \end{bmatrix} \begin{bmatrix} a_1 & 0 & \dots & 0 \\ 0 & a_2 & \dots & 0 \\ \dots & \dots & \dots & \dots \\ 0 & 0 & \dots & a_n \end{bmatrix}^{-1} \\ &= \eta C D^{-1} \end{aligned} \tag{4.15}$$

where $C = [c_{kj}]$ is the contact rate matrix. Thus, the basic reproduction number $\mathcal{R}_{0_p}$ in (4.6) becomes

$$\begin{aligned} \mathcal{R}_{0_p} &= \frac{\eta N \big(p(1-s_0^*) + s_0^*\big)}{\alpha} \rho\big(DCD^{-1}\big) \\ &= \frac{\eta N \big(p(1-s_0^*) + s_0^*\big)}{\alpha} \rho(C) \,, \end{aligned} \tag{4.16}$$

and the final size equation in (4.11) becomes

$$\log(\psi_k) = -\frac{\eta N}{\alpha} \sum_{j=1}^{n} c_{kj} \big(s_0^*(1-\psi_j) + (1-s_0^*)(1-\psi_j^p) \big) \,. \tag{4.17}$$

Contact group represents age group

To find the contact rate matrix C, we use the matrices K, P and $M(k,\ell)$ introduced in section 4.2. The total number of contacts of an individual in age group k and degree group ℓ with all other age and degree groups is $K_{k\ell} M(k,\ell)$. To restrict our model to age groups,

we sum the matrix $K_{k\ell}M(k,\ell)$ along the degree groups. Let $\vec{1} = (1,1,1,1,1)^t$. Thus, an individual in age group k and degree group ℓ has $K_{k\ell}M(k,\ell)\vec{1}$ contacts with all other age groups. The probability that an individual in age group k belongs to degree group ℓ is $\frac{P_{k\ell}}{\sum\limits_j P_{kj}}$. Summing across an individual's degree group, who belongs to contact group k and degree group ℓ, the contact rate from age group k to all other age groups is

$$\vec{c}_k = \sum_\ell \left[\frac{P_{k\ell}}{\sum\limits_j P_{kj}} K_{k\ell} M(k,\ell)\vec{1} \right],$$

which gives the 8×8 contact rate matrix $C = [\vec{c}_1, \vec{c}_2, \ldots, \vec{c}_8]$ in terms of matrices $M(k,\ell)$, K and P from the data as described in section 4.2.

Contact group represents age and degree group

In this case, we do not need to sum across the degree groups. Thus, an individual's contact rate from age group k and degree group ℓ to all other age and degree group is

$$\vec{c}_{8(\ell-1)+k} = \frac{P_{k\ell}}{\sum\limits_j P_{kj}} K_{k\ell} \vec{m}(k,\ell),$$

where $\vec{m}(k,\ell)$ is the column representation of the matrix $M(k,\ell)$, i.e., the $8(v-1)+u$ entry of $\vec{m}$ is the (u,v) entry of the matrix $M(k,\ell)$. The 40×40 contact rate matrix is found as $C = [\vec{c}_1, \vec{c}_2, \ldots, \vec{c}_{40}]$.

We use the matrix C and s_i^* to compute the basic reproduction number $\mathcal{R}_{0_p}$ of a future pandemic influenza from (4.16). Let $\frac{\eta N}{\alpha} = \delta$, a free parameter. For each value of $p \in [0,1]$, the range of $\delta \in [\delta_1(p), \delta_2(p)]$ is determined to make $\mathcal{R}_{0_p}$ of a future 1968-like pandemic influenza in the interval $[1.84, 2.59]$; see Table 3.3. Here, $\delta_1(p)$ corresponds to 1.84, and $\delta_2(p)$ corresponds to 2.59 for each value of p. Using δ, s_i^* and c_{kj}, the (k,j)th entry of C, we solve the non-linear system (4.17) to compute ψ_k for $k = 1, 2, \ldots, n$. The system (4.17) has a root $\psi_k = 1$, which is not biologically interesting, since $\psi_k = 1$ means there is no pandemic influenza in contact group k. For a biologically meaningful root, (4.17) is solved numerically by using fixed s_i^* and c_{kj} with $\delta = \delta_1(p)$ or $\delta_2(p)$. We find numerically that (4.17) has a unique root in the interior of $(0,1)^n$. We then compute the attack rate Z from (4.12) and plot it in Fig. 4.1.

The pandemic influenza model (4.2) requires the cross-immunity between the pandemic and seasonal subtype of influenza to be in the range 80–95% to observe a future 1968-like

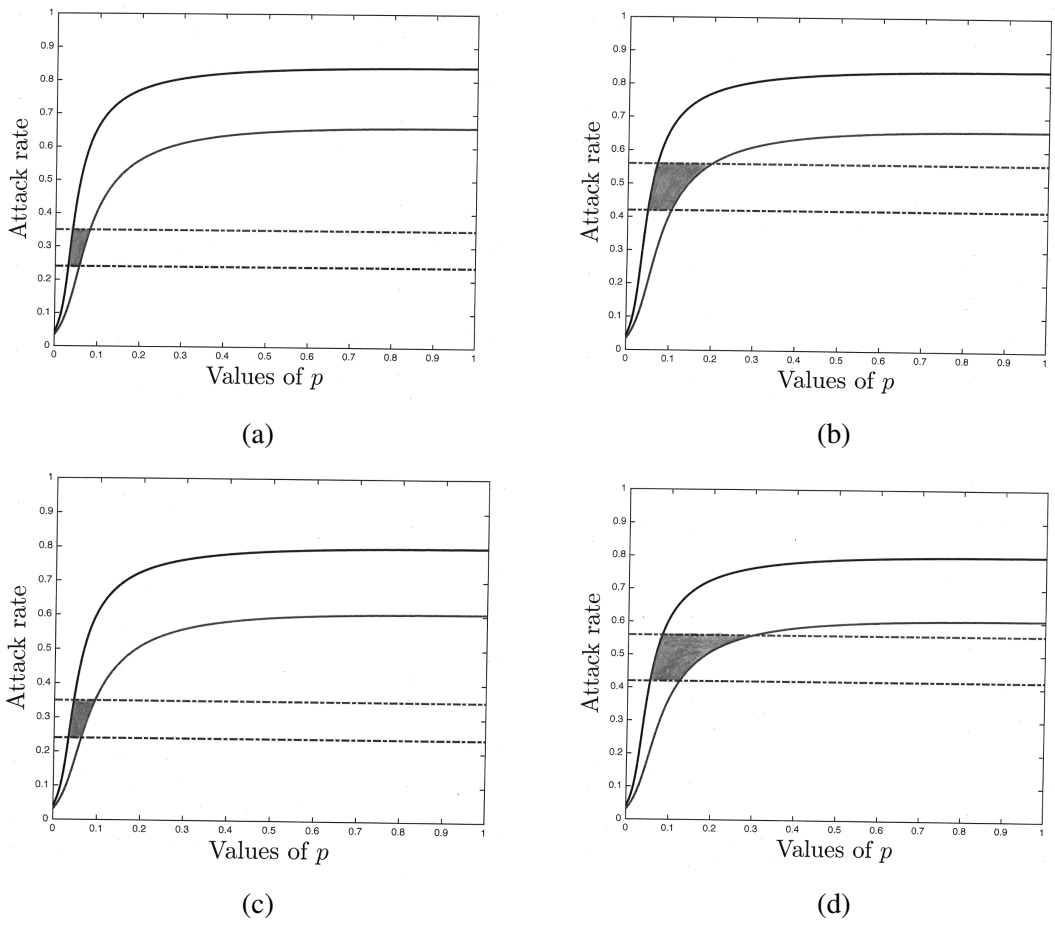

Figure 4.1: The solid lines represent the lower and upper bound of attack rates for $\delta \in [\delta_1(p), \delta_2(p)]$ from the model with constant susceptibility p. The horizonal lines are the lower and upper bound of symptomatic attack rate 24–35% in Fig. 4.1a and Fig. 4.1c, and serologically confirmed attack rate 42–56% in Fig. 4.1b and Fig. 4.1d. The contact group equals age group in Fig. 4.1a and Fig. 4.1b; it equals age and degree group in Fig. 4.1c and Fig. 4.1d. The parameter values corresponding to the shaded region between the horizontal lines give the pandemic attack rate in the observed range.

pandemic influenza with serologically confirmed attack rate 42–56% (Fig. 4.1b). Also, this range of cross-immunity is very high for the other cases in Fig. 4.1a, 4.1c and 4.1d. Kucharski et al. [56] found that the cross-immunity between two seasonal strains that appeared in two consecutive seasons is about 75%, but we found in chapter 3 that this cross-immunity is 88%. Since the pandemic subtype is a recombination of influenza subtypes, this high cross-immunity between influenza subtypes may be unrealistic.

4.4 Heterogeneous Mixing of Individuals with Infection History Dependent Susceptibility to the Pandemic

The heterogeneity in contact rate lowers the attack rate. But, to reach the observed attack rate, the model still requires unrealistically high cross-immunity. We now modify the pandemic influenza model in section 4.3.1 to incorporate infection history dependent susceptibility to the pandemic influenza. For this, we choose the model (4.2) over the model (4.13) since the model (4.2) keeps track of an individual's infection history, but assumes individuals in S_{ki} for $i \geq 1$ have susceptibility p to the pandemic influenza. We now assume that individuals in S_{ki} have susceptibility p_i to the pandemic influenza, with p_i following a monotonic relation to satisfy the fact that susceptibility increases with time between the last seasonal influenza infection and the pandemic infection. Keeping all other assumptions the same as in section 4.3.1, the transmission dynamics of the pandemic influenza evolves according to the following equations for $k = 1, 2, \ldots, n$

$$\frac{dS_{k0}}{dt} = -S_{k0} \sum_{j=1}^{n} \beta_{kj} I_j \,, \tag{4.18a}$$

$$\frac{dS_{ki}}{dt} = -p_i S_{ki} \sum_{j=1}^{n} \beta_{kj} I_j \,, \qquad i = 1, 2, \ldots, \tag{4.18b}$$

$$\frac{dI_k}{dt} = \big(\sum_{j=1}^{n} \beta_{kj} I_j\big)\big(\sum_{i=1}^{\infty} p_i S_{ki} + S_{k0}\big) - \alpha I_k \,, \tag{4.18c}$$

$$\frac{dR_k}{dt} = \alpha I_k \,. \tag{4.18d}$$

The initial conditions are $S_{ki}(0) = S_{ki}^*$ with $\sum_{k=1}^{n} \sum_{i=0}^{\infty} S_{ki}^* \approx N$, and $I_k(0)$ is small and positive and $R_k(0) = 0$.

Reproduction Number, Final Size Relation, and Attack Rate of the Pandemic

Following the calculations in section 4.3.1, the T matrix becomes $T = N\big(\sum_{i=1}^{\infty} p_i s_i^* + s_0^*\big) D$. Thus, the basic reproduction number $\mathcal{R}_{0_p}$ of the model (4.18) is given by

$$\mathcal{R}_{0_p} = \frac{\eta N\big(\sum_{i=1}^{\infty} p_i s_i^* + s_0^*\big)}{\alpha} \rho(C)$$

$$= \delta\big(\sum_{i=1}^{\infty} p_i s_i^* + s_0^*\big)\rho(C).$$

The final size relation and the attack rate of the pandemic influenza of the model (4.18) become

$$\log(\psi_k) = -\delta \sum_{j=1}^{n} c_{kj}\left[s_0^*(1-\psi_j) + \sum_{i=1}^{\infty} s_i^*(1-\psi_j^{p_i})\right], \tag{4.19}$$

and

$$Z = 1 - \sum_{k=1}^{n} a_k\big[s_0^*\psi_k + \sum_{i=1}^{\infty} s_i^*\psi_k^{p_i}\big]. \tag{4.20}$$

Numerical Simulation

To simulate the model (4.18), we assume p_i in the form $p_i = 1 - \xi q^i$, where $\xi \in [0,1]$ represents the cross-immunity between the pandemic influenza and seasonal strain of influenza that appeared before the pandemic outbreak. The cross-immunity q between seasonal strains of influenza is found to be $q = 0.88$; see Table 3.3. We compute the basic reproduction number $\mathcal{R}_{0_p}$ from (4.19) and final size from (4.19). We compute the attack rate Z from (4.20) and plot it in Fig. 4.2.

In order to observe a future 1968-like pandemic influenza with serologically confirmed attack rate 42–56%, the model (4.18) requires the cross-immunity in the range 98–100% (Fig. 4.2b) when the contact group equals the age group, and 78–100% (Fig. 4.2d) when the contact group equals the age group and degree group.

4.5 Discussion

The attack rate of pandemic influenza determines the average susceptibility of the population to a seasonal subtype after the pandemic. Our pandemic influenza model with homogeneous mixing of individuals fails to estimate parameter values in a reasonable range for the attack rate of a future 1968-like pandemic influenza. To overcome the shortcoming, we extend the pandemic model to incorporate the heterogeneity in contact rates of individuals in the dynamics of pandemic influenza. Our model uses the contact rate data from the Greater Vancouver Metropolitan area to determine the contact rate of an individual from one contact group to an individual in other contact group. The model

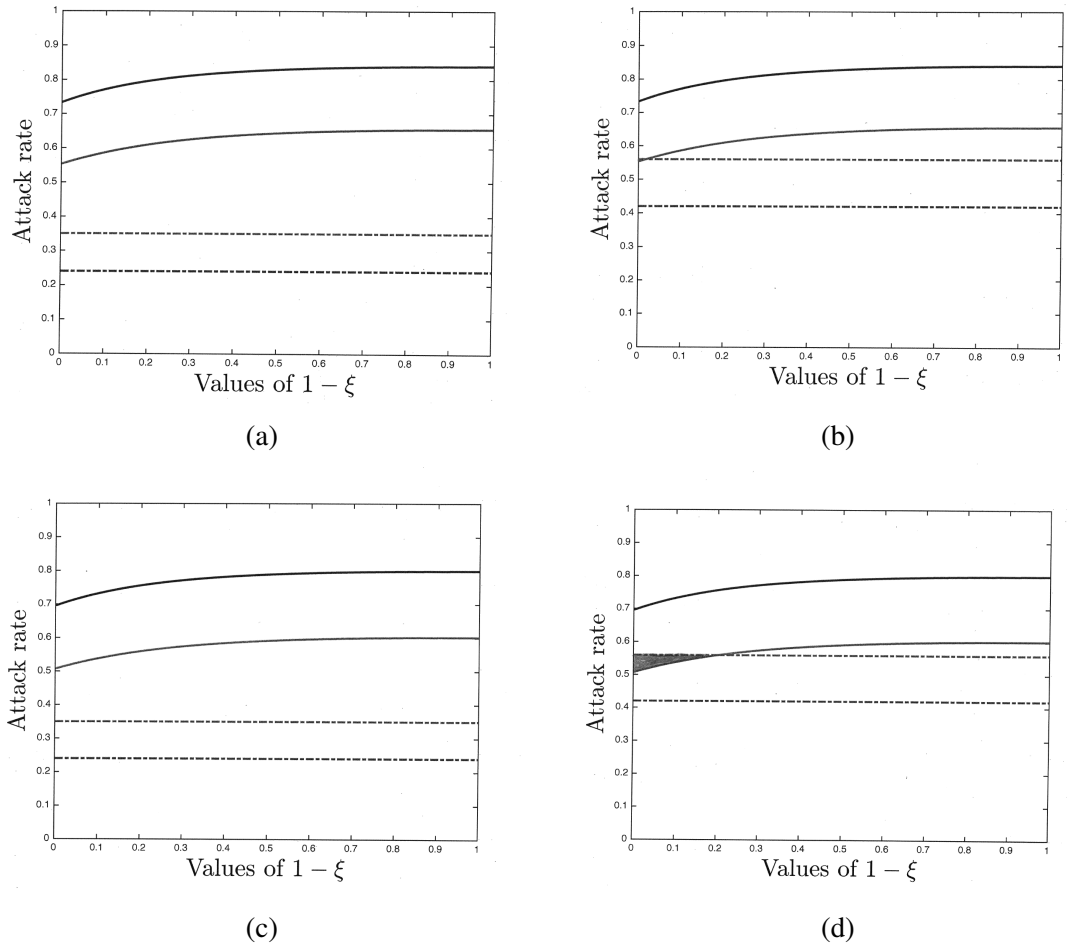

Figure 4.2: The solid lines represent the lower and upper bound of the attack rates for $\delta \in [\delta_1(\xi), \delta_2(\xi)]$ from the model with infection history dependent susceptibility p_i. The horizonal lines are the lower and upper bound of symptomatic attack rate 24–35% in Fig. 4.2a and Fig. 4.2c, and serologically confirmed attack rate 42–56% in Fig. 4.2b and Fig. 4.2d. The contact group equals age group in Fig. 4.2a and Fig. 4.2b; it equals age and degree group in Fig. 4.2c and Fig. 4.2d. The parameter values corresponding to the shaded region between the horizontal lines give the pandemic attack rate in the observed range.

requires the distribution of susceptible individuals in each contact group, as in chapter 2.

In our model, we considered the contact group is either age group or age and degree group. For the model with constant susceptibility to the pandemic influenza, when the contact group equals the age group, the cross-immunity between a future 1968-like pandemic and seasonal subtype is required to be 92–97% to observe the symptomatic attack rate 24–35% and the basic reproduction number $[1.84, 2.59]$. This range of cross-immunity lowers down to 80–95% for a 1968-like pandemic influenza with the observed serologically

confirmed attack rate 42–56%. When the contact group equals the age and degree group, the cross-immunity is required to be 91–97% for the observed symptomatic attack rate, and 70–95% for the observed serologically confirmed attack rate.

For the model with infection history dependent susceptibility, when the contact group equals the age group or age and degree group, the model gives the attack rate much higher than the observed symptomatic attack rate 24–35%, i.e., there is no parameter values for which our model estimates the observed symptomatic attack rate. However, the model gives parameter values for the observed serologically confirmed attack rate 42-56%. When the contact group equals the age group, the cross-immunity is required to be 98–100%, and when the contact group equals the age and degree group, the cross-immunity is required to be 78–100% for the observed serologically confirmed attack rate.

Our pandemic influenza model with infection history dependent susceptibility p_i assumes that an individual's susceptibility increases with the time between the last seasonal infection and the pandemic infection. Thus, the estimations of cross-immunity are higher than the estimations from the model with constant susceptibility p to the pandemic influenza. However, both models give parameter values that corresponds to unrealistically high cross-immunity between influenza subtypes. Since a genetic reassortment produces a pandemic subtype, and the cross-immunity between influenza strains is about 88% (chapter 3), it is very unlikely that the pandemic and seasonal subtype have cross-immunity at this high end. Thus, heterogeneity in contact rate cannot alone explain the dynamics of a future pandemic influenza that might have either a symptomatic attack rate 24–35% or serologically confirmed attack rate 42–56%.

Chapter 5

Conclusions

5.1 Replacement or Coexistence Condition Revisited

In chapter 2, we determine the condition of replacement or coexistence of a seasonal strain by the pandemic subtype, by assuming values of the parameters q, the cross-immunity between an influenza strain and its mutant, and $\mathcal{R}_0$, the basic reproduction number of seasonal influenza (see Fig. 2.4). In chapter 3, we find these parameters $q = 0.88\ (0.85 - 0.91)$ and $\mathcal{R}_0 = 2.15\ (1.84 - 2.59)$ for the influenza subtype H3N2. Using these parameter values, we now recompute Fig. 2.4 to determine the range of cross-immunity values for which influenza subtype H3N2 is replaced by or coexists with a future pandemic subtype of influenza.

The numerical simulation in section 2.3.2 assumes initial values right after the 1968 pandemic influenza by taking $S_i(0)$ such that $\sum_{i=1}^{n} S_i(0) \approx 1$. Davis et al. [28] (see section 3.2) found that the serologically confirmed attack rate of the 1968 pandemic influenza was 49%, thus we take $S_1(0) = 0.49$, $S_0(0) = 0.51$ and all other $S_i(0) = 0$ for $i \geq 2$, and find the equilibrium distribution S_i^* of susceptible individuals. Then the values of ψ in (2.9) is found from (2.6). Equation (2.6) requires the knowledge of the basic reproduction number $\mathcal{R}_{0_p}$ of a future pandemic influenza. Since $\mathcal{R}_{0_p}$ is not known, we take it equal to $\mathcal{R}_0$ of the 1968 pandemic influenza. Now for each value of $p \in [0, 1]$, we use the S_i^* values; compute the reproduction number $\mathcal{R}_s$ and plot it in Fig. 5.1.

Fig. 5.1 shows that a future 1968-like pandemic subtype of influenza requires a cross-immunity in the range 9–53$\%$ to replace the influenza subtype H3N2. We run the simulation for 200 times by choosing the parameters q, $\mathcal{R}_0$ and Z from a multivariate normal distribution, and find a slightly wider range 8–58$\%$ of cross-immunity to replace

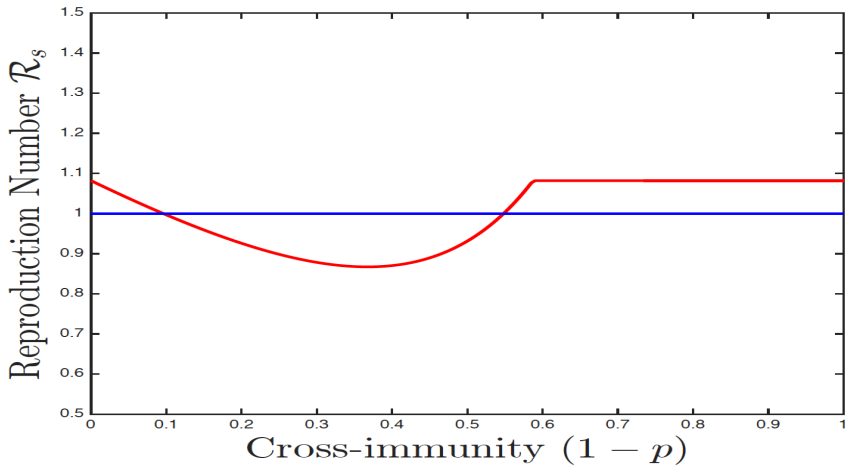

Figure 5.1: The curve $\mathcal{R}_s$ plotted as a function of cross-immunity $1-p$, giving the range of cross-immunity values for which the seasonal subtype H3N2 is replaced by a future pandemic subtype or reappears after the pandemic. The parameters are $\mathcal{R}_0 = 2.15$, $\mathcal{R}_{0_p} = 2.15$, $q = 0.88$. The threshold quantity $\mathcal{R}_s = 1$ is marked by a horizontal line, and the replacement range is determined by values of $\mathcal{R}_s$ below this line.

the influenza subtype H3N2 by a future pandemic subtype. Since the H1N1 pandemic influenza in 1977 did not replace the previous seasonal subtype H3N2, the cross-immunity between the two subtypes must be less than 9%.

5.2 Simplified Condition for Replacement or Coexistence

In section 2.3.2, we found that the fraction of individuals S_0^* who have never been infected by the seasonal influenza is approximately 5–6$\%$. Neglecting S_0^*, the reproduction number $\mathcal{R}_s$, in (2.9), of seasonal influenza after the pandemic becomes

$$\mathcal{R}_s = \mathcal{R}_0 \sum_{i=1}^{\infty} \tau_i S_i^* (\psi^p + p(1-\psi^p)) \,. \tag{5.1}$$

Before the pandemic outbreak, i.e., at the equilibrium, from (2.16), the reproduction number of seasonal influenza becomes

$$\mathcal{R}^* = \mathcal{R}_0 \sum_{i=1}^{\infty} \tau_i S_i^* \,. \tag{5.2}$$

The quantity $\mathcal{R}^*$ is the reproduction number of seasonal influenza, which takes the

cross-immunity into account (see section 2.2.3), and it has been estimated by many authors; for example, Chowell et al. [19] gives an estimated $\mathcal{R}^* = 1.3$ from a model with homogeneous mixing of individuals. Thus, using (5.2) in (5.1), the reproduction number $\mathcal{R}_s$ is given by

$$\mathcal{R}_s = \mathcal{R}^*(\psi^p + p(1 - \psi^p)) \,. \tag{5.3}$$

where ψ^p is related with the attack rate Z of the pandemic influenza by $Z = 1 - \psi^p$ from (2.8). Using Z, $\mathcal{R}_s$ in (5.3) is given by

$$\mathcal{R}_s = \mathcal{R}^*\big[1 - (1 - p)Z\big], \tag{5.4}$$

which is a linear equation in terms of p for a fixed value of Z.

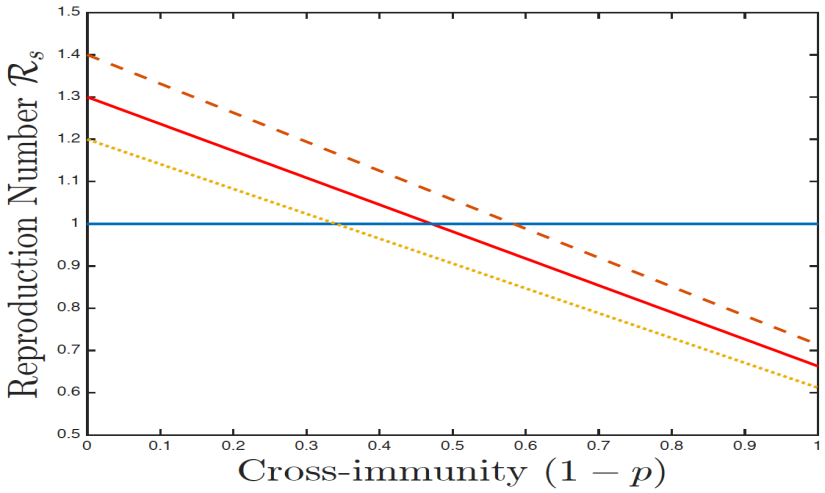

Figure 5.2: The curve $\mathcal{R}_s$ plotted as a function of cross-immunity $1 - p$. The attack rate Z of the pandemic is taken as $Z = 0.49$ and the reproduction number $\mathcal{R}^*$ of seasonal influenza is (a) $\mathcal{R}^* = 1.3$ (solid line), (b) $\mathcal{R}^* = 1.2$ (dotted line), (c) $\mathcal{R}^* = 1.4$ (dashed line). The threshold quantity $\mathcal{R}_s = 1$ is marked by a horizontal line, and the replacement range is determined by values of $\mathcal{R}_s$ below this line.

Since $Z = 0$ indicates that there is no outbreak of pandemic influenza, implying the existence of seasonal influenza, we analyze (5.4) for $Z \in (0, 1]$. Differentiating (5.4) with

respect to $\mathcal{R}^*$, $(1-p)$ and Z gives

$$\begin{aligned} \frac{\partial \mathcal{R}_s}{\partial \mathcal{R}^*} &= 1-\sigma Z > 0 \\ \frac{\partial \mathcal{R}_s}{\partial (1-p)} &= -\mathcal{R}^* Z < 0 \\ \frac{\partial \mathcal{R}_s}{\partial Z} &= -\mathcal{R}^* \sigma < 0 \end{aligned}$$

The reproduction number $\mathcal{R}_s$ of seasonal influenza after the pandemic increases with increasing $\mathcal{R}^*$ since $\frac{\partial \mathcal{R}_s}{\partial \mathcal{R}^*} > 0$. Thus, the coexistence of seasonal influenza becomes easier with increasing $\mathcal{R}^*$ (Fig. 5.2). However, the replacement of seasonal influenza becomes easier with increasing cross-immunity $1-p$ since $\frac{\partial \mathcal{R}_s}{\partial (1-p)} < 0$. (Fig. 5.2). Also, seasonal subtype replacement is easier with increasing attack rate Z since $\frac{\partial \mathcal{R}_s}{\partial Z} < 0$ (Fig. 5.3).

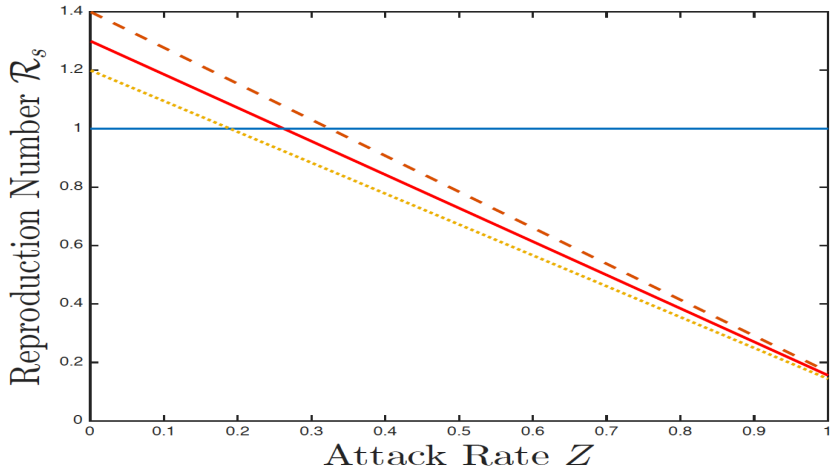

Figure 5.3: The curve $\mathcal{R}_s$ plotted as a function of attack rate Z of the pandemic influenza. The cross-immunity between the subtypes is taken as 88% from chapter 3 and the reproduction number $\mathcal{R}^*$ of seasonal influenza is (a) $\mathcal{R}^* = 1.3$ (solid line), (b) $\mathcal{R}^* = 1.2$ (dotted line), (c) $\mathcal{R}^* = 1.4$ (dashed line). The threshold quantity $\mathcal{R}_s = 1$ is marked by a horizontal line, and the replacement range is determined by values of $\mathcal{R}_s$ below this line.

The 1968 pandemic influenza

In section 5.1, we find that the outbreak of a future 1968-like pandemic influenza is cross-immunity dependent; it cannot invade if the cross-immunity between the subtypes is 60–100$\%$ (Fig. 5.1, horizontal line). However, when we neglect S_0^* (section 5.2), the

reproduction number $\mathcal{R}_s$, in (5.4), implies that there is an outbreak of pandemic influenza with the attack rate Z. Using $q = 0.88$ and $\mathcal{R}_0 = 2.15$ in (5.2), we compute $\mathcal{R}^* = 1.08$ by iterating our season-to-season mapping equations (see section 2.2.3) for the influenza subtype H3N2. We then use $\mathcal{R}^* = 1.08$ in (5.4), and compute $\mathcal{R}_s$ for fixed values of attack rate Z. The reproduction number $\mathcal{R}_s$ of seasonal influenza is plotted in Fig. 5.4 to determine the range of cross-immunity for which H3N2 is replaced by a future 1968-like pandemic subtype of influenza.

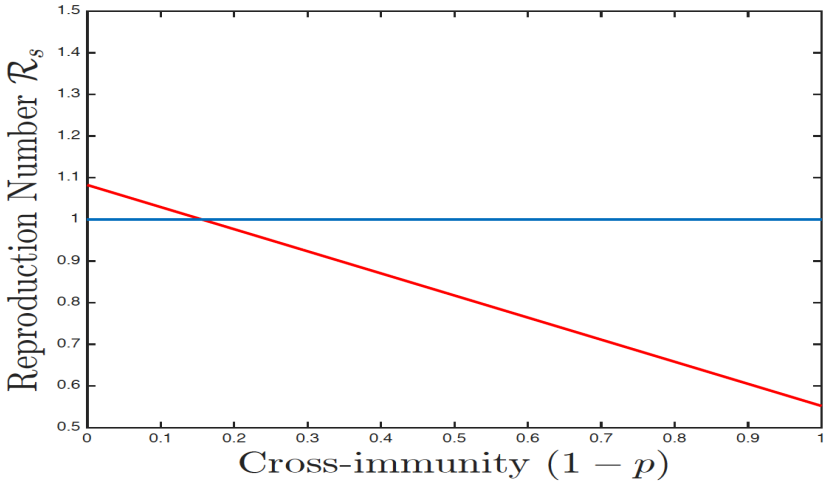

Figure 5.4: The curve $\mathcal{R}_s$ plotted as a function of cross-immunity $1-p$. The threshold quantity of reproduction number is marked by a horizontal line. The parameters are $\mathcal{R}_0 = 2.15, q = 0.88$ and $Z = 0.49$.

5.3 Discussion and Future Directions

We investigate the mechanisms of interaction between subtypes: why there have been two replacement of subtypes (e.g., H1N1 by H2N2 and H2N2 by H3N2) and one coexistence of subtypes (e.g., H3N2 and H1N1) by formulating a hybrid model for influenza A epidemics. Qualitatively, our hybrid model shows that the replacement of seasonal subtype by the pandemic subtype happens at intermediate levels of cross-immunity between the subtypes. Quantitatively, this cross-immunity is found to be 9–53$\%$ to replace a seasonal subtype by a future 1968-like pandemic influenza.

Since there was replacement of influenza subtype H1N1 by the subtype H2N2 in 1957, and influenza subtype H2N2 by the subtype H3N2 in 1968, according to our model, the

cross-immunity between H1N1 and H2N2, and between H2N2 and H3N2 must be in the range 9–53$\%$ (Fig. 5.1). The pandemic subtypes H2N2 and H3N2 were a reassortment of gene segments from human influenza viruses with avian influenza viruses [10]. The subtype H2N2 derived five genes from the human H1N1 seasonal influenza, and H3N2 derived six genes from the previous H2N2 seasonal influenza [78]; thus the range 9-53$\%$ of cross-immunity between the subtypes is reasonable. On the other hand, according to our model, the cross-immunity between the subtypes H1N1 and H3N2 in 1977 must be less than 9$\%$ (neglecting S_0^*, this cross-immunity is $< 16\%$) for the coexistence of subtypes. This weak cross-immunity between the subtypes was due to the fact that the subtype H1N1 was not directly descended from the subtype H3N2 in 1977.

If we take the cross-immunity between H1N1 and H2N2 to equal $a \in [0.09, 0.53]$, and the cross-immunity between H2N2 and H3N2 to equal $b \in [0.09, 0.53]$, then for the coexistence of subtypes H1N1 and H3N2 in 1977, the cross-immunity must satisfy $ab < 0.09$ (neglecting S_0^*, $ab < 0.16$); thus the cross-immunity between H1N1 and H2N2, and between H2N2 and H3N2 is at best 30% (neglecting S_0^*, 40%). Our findings also suggest that the estimated reproduction number of seasonal influenza $\mathcal{R}^* = 1.3$ could be an overestimation. Because, in order to replace a seasonal subtype with reproduction number $\mathcal{R}^* = 1.3$, a future 1968-like pandemic influenza requires 47–100$\%$ cross-immunity between the subtypes (Fig. 5.2).

Our hybrid model (see chapter 2) assumes that the pandemic subtype survives in the season following the pandemic, but we do not address what mechanism helps the pandemic subtype to become seasonal. In the last century, a large fraction of individuals gained cross-immunity against the pandemic subtype since the attack rate of the pandemic influenza was much higher than the attack rate of the seasonal influenza. Despite this large population level cross-immunity, the pandemic influenza caused an outbreak in the season following the pandemic. Further investigation is required to understand the mechanism that helps the pandemic subtype invade in the next season. Also, the model takes account of only the season following a pandemic. If both subtypes coexist in that season, then understanding the interaction and competition between the two subtypes in subsequent seasons requires further modeling.

Our hybrid model (see chapter 2) is based on the assumption of homogeneous mixing of the whole population. In chapter 4, we incorporated inhomogeneous mixing of individuals in the dynamics of pandemic influenza. Future models may incorporate inhomogeneous mixing of individuals in the dynamics of seasonal influenza to investigate whether it changes the conditions found from the hybrid model with homogeneous mixing

of individuals.

Our novel statistical method (see chapter 3) finds the cross-immunity between influenza strains incorporating susceptibility of individuals depending on the evolutionary tree of antigens of influenza H3N2. Our method suggests that the 1969 and 1971 strains are two different branches of the 1968 strain. But in our hybrid model, we assume that the individuals' infection history is linear following Andreasen's seasonal model. Future models may incorporate individuals' infection history based on the evolutionary tree of antigens to find a condition for the replacement or coexistence of a seasonal subtype.

Our pandemic model (see chapter 4) with heterogeneity in contact rate cannot alone explain the low attack rate of the pandemics. He et al. [48] showed that the three waves of the 1918 pandemic influenza might have resulted due to the factors–(i) schools opening and closing, (ii) temperature changes during the outbreak, and (iii) behavioural change in human response to the outbreak; of which behavioural change had the largest effect. Thus, future models may investigate whether seasonal change in transmission rate or behavioral change of individuals during the pandemic could explain the low attack rate of the pandemics in the last century.

Appendix A

Symbol	Meaning
t_s	Duration of seasonal epidemics
t_b	Beginning time of the pandemic influenza
t_e	Ending time of the pandemic influenza
S	Fraction of susceptible individuals who escaped the pandemic
$\tilde{S}$	Fraction of susceptible individuals who recovered from the pandemic
I	Fraction of infected and infectious individuals
R	Fraction of recovered individuals
$S_0, \tilde{S}_0$	Fraction of susceptible individuals in S, $\tilde{S}$ who have never been infected by seasonal subtypes
$S_i, \tilde{S}_i$	Fraction of susceptible individuals in S, $\tilde{S}$ who were infected i seasons ago for $i \geq 1$
S_0^*, S_i^*	Fraction of susceptible individuals at equilibrium in S_0 and S_i for $i \geq 1$
s_ℓ^c	Fraction of susceptible individuals at the end of the current season c who had their last influenza A/H3N2 in season ℓ
s_0^c	Fraction of susceptible individuals at the end of the current season c who have never been infected by the influenza A/H3N2
i, r	Fraction of infectious, and recovered individuals in current season c who had their last influenza A/H3N2 in season ℓ
τ_i	Fraction of susceptibility of individuals in S_i to seasonal influenza
$p\tau_i$	Fraction of susceptibility of individuals in $\tilde{S}_i$ to seasonal influenza
τ_ℓ^c	Susceptibility of individuals in S_ℓ^c
q	Probability of antibodies from the previous year's strain binding to the current seasonal strain of influenza
$1-p$	Cross-immunity between the pandemic subtype and any seasonal strain
α	Recovery rate for seasonal influenza
β_s	Transmission rate of seasonal influenza
d	Natural death rate of individuals
$d(c,\ell)$	Antigenic distance between the nodes c and ℓ on the evolutionary tree of antigens
$\mathcal{R}_0$	Basic reproduction number of seasonal influenza
$\mathcal{R}_{0_p}$	Basic reproduction number of the pandemic influenza
$\mathcal{R}_s$	Reproduction number of seasonal influenza after the pandemic
ψ	Fraction of susceptible individuals who have never been infected by the seasonal influenza and escaped the pandemic infection
ϕ	Fraction of susceptible individuals who have never been infected by the seasonal influenza and escaped seasonal influenza in the current season
ϕ_ℓ^c	Fraction of individuals in S_ℓ^c who escaped influenza infection during the season c
A^{68}	Attack rate of the 1968 pandemic
ϵ	Vaccine protection against the vaccinating strain

Bibliography

[1] B. Adams and A. Sasaki. Cross-immunity, invasion and coexistence of pathogen strains in epidemiological models with one-dimensional antigenic space. *Math. Biosciences*, 210:680–699, 2007.

[2] B. Adams and A. Sasaki. Antigenic distance and cross-immunity, invasibility and coexistence of pathogen strains in an epidemiological model with discrete antigenic space. *Theor. Popl. Biol*, 76:157–167, 2009.

[3] R. M. Anderson and R. M. May. *Infectious Diseases of Humans: Dynamics and Control*. Oxford University, Oxford, 1991.

[4] V. Andreasen. Dynamics of annual influenza A epidemics with immuno-selection. *J. Math. Biol*, 46:504–536, 2003.

[5] V. Andreasen, J. Lin, and S. A. Levin. The dynamics of co-circulating influenza strains conferring partial cross-immunity. *J. Math. Biol*, 35:825–842, 1997.

[6] R. Antia, R. R. Regoes, J. C. Koella, and C. T. Bergstrom. The role of evolution in the emergence of infectious diseases. *Nature*, 426:658–661, 2006.

[7] S. M. Asaduzzaman, Junling Ma, and P. van den Driessche. The coexistence or replacement of two subtypes of influenza. *Math. Biosci.*, 270:1–9, 2015.

[8] L. J. Bain and M. Engelhardt. *Introduction to Probability and Mathematical Statistics*. Duxbury Press, 2nd edition, 2000.

[9] F. Ball. Deterministic and stochastic epidemics with several kinds of susceptibles. *Adv. Appl. Probab.*, 17:1–22, 1985.

[10] W. Bean, M. Schell, J. Katz, Y. Kawaoka, C. Naeve, O. Gorman, and W. G. Webster. Evolution of the H3 influenza virus hemagglutinin from human and nonhuman hosts. *J. Virology*, 66:1129–1138, 1992.

[11] M. Biggerstaff, S. Cauchemez, C. Reed, M. Gambhir, and L. Finelli. Estimates of the reproduction number for seasonal, pandemic and zoonotic influenza: a systematic review of the literature. *BMC Infectious Diseases*, 14:480, 2014.

[12] M. F. Boni, J. R. Gog, V. Andreasen, and F. B. Christiansen. Influenza drift and epidemic size: the race between generating and escaping immunity. *Theor. Popul. Biol.*, 65(2):179–191, 2004.

[13] M. F. Boni, J. R. Gog, V. Andreasen, and M. W. Feldman. Epidemic dynamics and antigenic evolution in a single season of influenza A. *Proc. R. Soc. B*, 273:1307–1316, 2006.

[14] F. Brauer. Epidemic models with heterogeneous mixing and treatment. *Bulletin Math. Biol.*, 70:1869–1885, 2008.

[15] I. H. Brown. The epidemiology and evolution of influenza viruses in pigs. *Vet. Microbiol.*, 74:29–46, 2000.

[16] R. M. Bush, W. M. Fitch, C. A. Bender, and N. J. Cox. Positive selection on the H3 hemagglutinin gene of human influenza virus A. *Mol. Biol. Evol.*, 16(11):1457–1465, 1999.

[17] C. Castillo-Chavez, H. W. Hethcote, V. Andreasen, S. A. Levin, and W. M. Liu. Epidemiological models with age structure, proportionate mixing and cross-immunity. *J. Math. Biol.*, 27:233–258, 1989.

[18] S. Cauchemez, N. M. Ferguson, C. Wachtel, A. Tegnell, G. Saour, B. Duncan, and A. Nicoll. Closure of schools during an influenza pandemic. *Lancet Infectious Diseases*, 9(8):473–481, 2009.

[19] G. Chowell, M. A. Miller, and C. Viboud. Seasonal influenza in the United States, France, and Australia: transmission and prospects for control. *Epidemiology and Infection*, 136(6):852–864, 2008.

[20] J. M. Conway, A. R. Tuite, D. N. Fisman, and N. Hupert et al. Vaccination against 2009 pandemic H1N1 in a population dynamical model of Vancouver, Canada: timing is everything. *BMC Public Health*, 11(1):932, 2011.

[21] B. S. Cooper, R. J. Pitman, W. J. Edmunds, and N. J. Gay. Delaying the international spread of pandemic influenza. *PLoS Medicine*, 3(6):e212, 2006.

[22] R. B. Couch, W. A. Keitel, and T. R. Cate. Prevention of influenza virus infections by current inactivated influenza vaccines. In L. E. Brown, A. W. Hampson, and R. G. Webster, editors, *Options for the control of influenza III.* Amsterdam, Netherlands; Elsevier, 1996.

[23] B. Cowling, L. Lau, P. Wu, H. Wong, V. Fang, S. Riley, and H. Nishiura. Entry screening to delay local transmission of 2009 pandemic influenza A (H1N1). *BMC Infectious Diseases*, 10(1):82, 2010.

[24] N. J. Cox and C. A. Bender. The molecular epidemiology of influenza viruses. *Semin. Virol.*, 6:359–370, 1995.

[25] N. J. Cox and K. Subbarao. Influenza. *Lancet*, 354:1277–1282, 1999.

[26] N. J. Cox and K. Subbarao. Global epidemiology of influenza: past and present. *Annu. Rev. Med.*, 51:407?421, 2000.

[27] F. M. Davenport. Current knowledge of influenza vaccine. *JAMA*, 182:11–13, 1962.

[28] L. E. Davis, G. G. Caldwell, R. E. Lynch, R. E. Bailey, and T. D. Y. Chin. Hong Kong influenza: The epidemiologic features of a high school family study analyzed and compared with a similar study during the 1957 Asian influenza epidemic. *Am. J. Epidemiology*, 92(4):240–247, 1970.

[29] T. Day, J. B. Andre, and A. Park. The evolutionary emergence of pandemic influenza. *Proc. R. Soc. B*, 273:2945–2953, 2006.

[30] J. C. de Jong, G. F. Rimmelzwaan, R. A. Fouchier, and A. D. Osterhaus. Influenza virus: a master of metamorphosis. *J. Infection*, 40(3):218–228, 2000.

[31] O. Diekmann and J. A. P. Heesterbeek. *Mathematical Epidemiology of Infectious Diseases: Model Building, Analysis and Interpretation*. John Wiley & Sons, West Sussex, England, 2000.

[32] J. Dushoff, J. B. Plotkin, S. A. Levin, and D. J. D. Earn. Dynamical resonence can account for seasonality of influenza epidemics. *Proc. Nat. Aca. Sci.*, 101(48):16915–16916, 2004.

[33] J. Dushoff, J. B. Plotkin, C. Viboud, D. J. Earn, and L. Simonsen. Mortality due to influenza in the United States–an annualized regression approach using multiple-cause mortality data. *Am J. Epidemiol.*, 163(2):181–187, 2006.

[34] D. Earn, J. Dushoff, and S. A. Levin. Ecology and evolution of the flu. *Trends in Ecology and Evolution*, 17(7):334–340, 2002.

[35] N. M. Ferguson, D. Cummings, S. Cauchemez, C. Fraser, S. Riley, A. Meeyai, S. Iamsirithaworn, and D. S. Burke. Strategies for containing an emerging influenza pandemic in Southeast Asia. *Nature*, 437:209–214, 2005.

[36] N. M. Ferguson, D. Cummings, C. Fraser, J. Cajka, P. Cooley, and D. Burke. Strategies for mitigating an influenza pandemic. *Nature*, 442(27):448–452, 2006.

[37] N. M. Ferguson, A. P. Galvani, and R. M. Bush. Ecological and immunological determinants of influenza evolution. *Nature*, 422:422–433, 2003.

[38] W. M. Fitch, J. E. Leiter, X. Li, and P. Palese. Positive Darwinian evolution in human influenza A viruses. *Proc. Natl. Acad. Sci.*, 88:4270–4274, 1991.

[39] H. M. Foy, M. K. Cooney, and R. McMahan. A Hong Kong influenza immunity three years after immunization. *JAMA*, 226(7):758–761, 1973.

[40] H. M. Foy, M. K. Cooney, R. McMahan, E. Bor, and J. T. Grayston. Single dose monovalent A/Hong Kong influenza vaccine efficacy 14 months after immunization. *JAMA*, 217(8):1067–1071, 1971.

[41] R. Gani, H. Hughes, D. Fleming, T. Griffin, J. Medlock, and S. Leach. Potential impact of antiviral drug use during influenza pademic. *Emerg. Infec. Diseases*, 11(9):1355–1361, 2005.

[42] P. W. Gill and A. M. Murphy. Naturally acquired immunity to influenza type A: a clinical and laboratory study. *Med. J. Australia*, 2(9):329–333, 1976.

[43] K. Glass and B. Barnes. How much would closing schools reduce transmission during an influenza pandemic? *Epidemiology*, 18(5):623–628, 2007.

[44] M. G. Gomes, G. F. Medley, and D. J. Nokes. On the determinants of population structure in antigenically diverse pathogens. *Proc. R. Soc. B*, 269:227–233, 2002.

[45] L. Greenberg and C. Normandin. Disparities in life expectancy at birth. Technical Report 82-624-X, Statistics Canada, April 2011.

[46] M. E. Halloran, I. M. Longini Jr., and C. J. Struchiner. *Design and Analysis of Vaccine Studies*. Springer, 2010.

[47] T. Harimoto, E. Rivera, J. Pearson, D. Senne, S. Krauss, Y. Kawaoka, and R. G. Webster. Origin and moleculer changes associated with emergence of a highly pathogenic H5N2 influenza virus in Mexico. *J. Virology*, 213(1):223–230, 1995.

[48] D. He, J. Dushoff, T. Day, J. Ma, and D. Earn. Inferring the causes of the three waves of the 1918 influenza pandemic in England and Wales. *Proc. R. Soc. B*, 280:20131345, 2013.

[49] V. S. Hinshaw, W. J. Bean, P. Fiorelli, G. Early, J. R. Geraci, and R. G. Webster. Characterization of two influenza A viruses from a pilot whale. *J. Virology*, 58(2):655–656, 1986.

[50] V. S. Hinshaw, W. J. Bean, R. G. Webster, J. E. Rehg, P. Fiorelli, G. Early, J. R. Geraci, and D. J. St. Aubin. Are seals frequently infected with avian influenza viruses? *J. Virology*, 53(3):863–865, 1984.

[51] C. Hsu and H. Shih. Transmission and control of an emerging influenza pandemic in a small-world airline network. *Accident Analysis and Prevention*, 42(1):93–100, 2010.

[52] C. Jackson, E. Vynnycky, and P. Mangtani. Estimates of the transmissibility of the 1968 (Hong Kong) influenza pandemic: evidence of increased transmissibility between successive waves. *Am. J. Epidemiol.*, 171:465–478, 2010.

[53] W. O. Kermack and A. G. McKendrick. A contribution to the mathematical theory of epidemics. *Proc. R. Soc. Lond.*, 115:700–721, 1927.

[54] W. O. Kermack and A. G. McKendrick. Contribution to the mathematical theory of epidemics, part. ii. *Proc. R. Soc. Lond.*, 138:55–83, 1932.

[55] W. O. Kermack and A. G. McKendrick. Contributions to the mathematical theory of epidemics, part. iii. *Proc. R. Soc. Lond.*, 141:94–112, 1932.

[56] A. J. Kucharski, J. Lessler, J. M. Read, H. Zhu, C. Q. Jiang, Y. Guan, D. A. T. Cummings, and S. Riley. Estimating the life course of influenza A (H3N2) antibody response from cross-sectional data. *PLOS Biology*, 13(3):e1002082, 2015.

[57] J. Lin, V. Andreasen, and S. A. Levin. Dynamics of influenza A drift: the linear three-strain model. *Math. Biosciences*, 162:33–51, 1999.

[58] I. M. Longini, M. E. Halloran, A. Nizam, and Y. Yang. Containing pandemic influenza with antiviral agents. *Am. J. Epidemiol.*, 159:623–633, 2004.

[59] I. M. Longini, A. Nizam, S. Xu, K. Ungchusak, W. Hanshaoworakul, D. Cummings, and M. E. Halloran. Containing pandemic influenza at the source. *Science*, 309:1083–1087, 2005.

[60] L. Meyers, B. Pourbohloul, M. Newman, D. Skowronski, and R. Brunham. Network theory and SARS: predicting outbreak diversity. *J. Theor. Biol.*, 232:71–81, 2005.

[61] C. M. Pease. An evolutionary epidemiological mechanism, with application to type A influenza. *Theor. Popul. Biol.*, 31:422–452, 1987.

[62] C. W. Potter. Determinants of immunity to influenza infection in man. *British Med Bull*, 35:69–75, 1979.

[63] S. Quach, J. Hamid, J. Pereira, C. Heidebrecht, and D. Shelley et al. Influenza vaccination coverage across ethnic groups in Canada. *CMAJ*, 184(15):1673–1681, 2012.

[64] S. Schoenbaum. Impact of influenza in persons and populations. In L. E. Brown, A. W. Hampson, and R. G. Webster, editors, *Options for the control of influenza III*. Amsterdam, Netherlands; Elsevier, 1996.

[65] C. Scholtissek, H. Burger, P. A. Bachmann, and C. Hannoun. Genetic relatedness of hemagglutinins of the H1 subtype of influenza A viruses isolated from swine and birds. *J. Virology*, 129(2):521–523, 1983.

[66] C. Scholtissek and E. Naylor. Fish farming and influenza pandemics. *Nature*, 331:215–215, 1988.

[67] J. L. Schulman and E. D. Kilbourne. Airborne transmission of influenza virus infection in mice. *Nature*, 195:1129–1130, 1962.

[68] R. Serfling. Methods for current statistical analysis of excess pneumonia-influenza deaths. *Public Health Reports*, 78:494?506, 1963.

[69] D. J. Smith, A. S. Lapedes, J. C. de Jong, T. M. Bestebroer, G. F. Rimmelzwaan, A. D. M. E. Osterhaus, and R. A. M. Fouchier. Mapping the antigenic and genetic evolution of influenza virus. *Science*, 305(5682):371–376, 2004.

[70] J. K. Taubenberger and D. M. Morens. 1918 influenza: the mother of all pandemics. *Emerging Infectious Diseases*, 12(1):15–22, 2006.

[71] J. K. Taubenberger, A. H. Reid, and T. G. Fanning. The 1918 influenza virus: a killer comes into view. *Virology*, 274:241–245, 2000.

[72] J. K. Taubenberger, A. H. Reid, A. E. Krafft, K. E. Bijwaard, and T. G. Fanning. Initial genetic characteristic of the 1918 "spanish" influenza virus. *Science*, 275:1793–1796, 1997.

[73] J. K. Taubenberger, A. H. Reid, R. M. Lourens, R. Wang, G. Jin, and T. G. Fanning. Characterization of the 1918 influenza virus polymerase gene. *Nature*, 437:889–893, 2005.

[74] J. J. Treanor, H. K. Talbot, S. E. Ohmit, L. A. Coleman, M. G. Thompson, et al. Effectiveness of seasonal influenza vaccines in the United States during a season with circulation of all three vaccine strains. *Clinical Infectious Diseases*, 55(7):951–959, 2012.

[75] P. van den Driessche and J. Watmough. Reproduction numbers and sub-threshold endemic equilibria for compartmental models of disease transmission. *Math. Biosci.*, 180:29–48, 2002.

[76] C. Viboud, R. F. Grais, B. A. P. Lafont, M. A. Miller, and L. Simonsen. Multinational impact of the 1968 Hong Kong influenza pandemic: evidence for a smoldering pandemic. *J. Infectious Diseases*, 192(2):233–248, 2005.

[77] R. G. Webster. Influenza: an emerging disease. *Emerging Infectious Diseases*, 4(3):436–441, 1998.

[78] R. G. Webster, W. J. Bean, O. T. Gorman, T. M. Chambers, and Y. Kawaoka. Evolution and ecology of influenza A viruses. *Microbiological Reviews*, 56(1):152–179, 1992.

[79] R. G. Webster, M. A. Yakhno, V. Hinshaw, W. J. Bean, and K. C. Murti. Intestinal influenza: replication and characterization of influenza viruses in ducks. *J. Virology*, 84(2):268–278, 1978.

[80] X. Yu, T. Tsibane, P. A. McGraw, F. S. House, and C. J. Keefer et al. Neutralizing antibodies derived from the B cells of 1918 influenza pandemic survivors. *Nature*, 455:532–536, 2008.

[81] X. S. Zhang, D. De Angelis, P. J. White, A. Charlett, R. G. Pebody, and J. McCauley. Co-circulation of influenza A virus strains and emergence of pandemic via reassortment: the role of cross-immunity. *Epidemics*, 5:20–33, 2013.